Research Paper

Brain and Neuroscience Advances

Brain and Neuroscience Advances
Volume 1: 1–21

DOI: 10.1177/2398212817739433
journals.sagepub.com/home/bna
SAGE

Combined allelic dosage of *Nfia* and *Nfib* regulates cortical development

Jens Bunt[1], Jason M Osinski[2], Jonathan WC Lim[1], Diana Vidovic[3], Yunan Ye[1], Oressia Zalucki[3], Timothy R O'Connor[4], Lachlan Harris[3], Richard M Gronostajski[2], Linda J Richards[1,3] and Michael Piper[1,3]

Abstract

Background: Nuclear factor I family members nuclear factor I A and nuclear factor I B play important roles during cerebral cortical development. Nuclear factor I A and nuclear factor I B regulate similar biological processes, as their expression patterns, regulation of target genes and individual knockout phenotypes overlap. We hypothesised that the combined allelic loss of *Nfia* and *Nfib* would culminate in more severe defects in the cerebral cortex than loss of a single member.

Methods: We combined immunofluorescence, co-immunoprecipitation, gene expression analysis and immunohistochemistry on knockout mouse models to investigate whether nuclear factor I A and nuclear factor I B function similarly and whether increasing allelic loss of *Nfia* and *Nfib* caused a more severe phenotype.

Results: We determined that the biological functions of nuclear factor I A and nuclear factor I B overlap during early cortical development. These proteins are co-expressed and can form heterodimers *in vivo*. Differentially regulated genes that are shared between *Nfia* and *Nfib* knockout mice are highly enriched for nuclear factor I binding sites in their promoters and are associated with neurodevelopment. We found that compound heterozygous deletion of both genes resulted in a cortical phenotype similar to that of single homozygous *Nfia* or *Nfib* knockout embryos. This was characterised by retention of the interhemispheric fissure, dysgenesis of the corpus callosum and a malformed dentate gyrus. Double homozygous knockout of *Nfia* and *Nfib* resulted in a more severe phenotype, with increased ventricular enlargement and decreased numbers of differentiated glia and neurons.

Conclusion: In the developing cerebral cortex, nuclear factor I A and nuclear factor I B share similar biological functions and function additively, as the combined allelic loss of these genes directly correlates with the severity of the developmental brain phenotype.

Keywords

Nuclear factor I, nuclear factor I A, nuclear factor I B, neocortex, hippocampus, cortical development, corpus callosum

Received: 12 June 2017; accepted: 1 October 2017

Introduction

The nuclear factor I (NFI) family of transcription factors play major roles during embryogenesis. Nuclear factor I-A (NFIA) and nuclear factor I-B (NFIB) are important for normal cortical development, as knockout of either *Nfia* or *Nfib* in mice results in very similar brain phenotypes, including dysgenesis of the corpus callosum, the disruption of midline fusion, enlarged ventricles and malformation of the hippocampus (Das Neves et al., 1999; Gobius et al., 2016; Piper et al., 2010; Shu et al., 2003; Steele-Perkins et al., 2005). Similarly, mutations or deletions of *NFIA* and *NFIB* in human patients with intellectual disability are associated with severe brain phenotypes, including dysgenesis of the corpus callosum, macrocephaly and enlarged ventricles (Gobius et al., 2016; Koehler et al., 2010; Lu et al., 2007; Negishi et al., 2015; Sajan et al., 2013).

Analyses of knockout mouse models suggest that the general underlying cause of these phenotypes is a cellular differentiation defect which affects radial glia, the embryonic neural progenitor cells of the cerebral cortex, which give rise to mature neurons

[1]The Queensland Brain Institute, The University of Queensland, Brisbane, QLD, Australia
[2]Department of Biochemistry, Program in Genetics, Genomics and Bioinformatics, Center of Excellence in Bioinformatics and Life Sciences, State University of New York at Buffalo, Buffalo, New York, USA
[3]The School of Biomedical Sciences, Faculty of Medicine, The University of Queensland, Brisbane, QLD, Australia
[4]School of Chemical and Molecular Biosciences and Institute for Molecular Bioscience, The University of Queensland, Brisbane, QLD, Australia

Corresponding authors:
Jens Bunt, The Queensland Brain Institute, The University of Queensland, QBI Building 79, Brisbane, QLD 4072, Australia.
Email: j.bunt@uq.edu.au

Linda J Richards, The Queensland Brain Institute, The University of Queensland, QBI Building 79, Brisbane, QLD 4072, Australia.
Email: richards@uq.edu.au

Michael Piper, The School of Biomedical Sciences, Faculty of Medicine, The University of Queensland, Brisbane, QLD 4072, Australia.
Email: m.piper@uq.edu.au

and glia in the cortex (Barry et al., 2008; Betancourt et al., 2014; Gobius et al., 2016; Piper et al., 2009, 2010, 2014). Knockout of either *Nfia* or *Nfib* causes the radial glia to remain proliferative and undifferentiated for an extended period of time. As a result, the generation of differentiated cellular progeny in the cortex is delayed (Barry et al., 2008; Gobius et al., 2016; Shu et al., 2003), a phenotype that is also observed in the cerebellum and the spinal cord (Deneen et al., 2006; Glasgow et al., 2013; Kilpatrick et al., 2012).

NFIA and NFIB proteins share highly homologous DNA-binding domains (Gronostajski, 2000) and have nearly identical DNA-binding motifs (Jolma et al., 2013). In the context of the brain, NFIA and NFIB share many common transcriptional downstream targets, including *Gfap*, *Hes1*, *Hes5*, *Sox3*, *Fgf9*, *Gli3*, *Id4*, *Cntn2*, *Efnb1* and *Cdh2* (Barry et al., 2008; Betancourt et al., 2014; Brun et al., 2009; Cebolla and Vallejo, 2006; Harris et al., 2016; Piper et al., 2009, 2010, 2014; Wang et al., 2007, 2010). *In vitro* experiments for targets such as *Gfap* and *Cntn2* have validated their direct regulation by both NFIA and NFIB. In contrast, transcriptional targets identified outside the central nervous system, such as *IGFBP5*, *PPARγ*, *C/EBPα*, *FABP4*, *BRN2* and *NKX3.1* (Fane et al., 2017; Grabowska et al., 2014; Perez-Casellas et al., 2009; Waki et al., 2011), are differentially regulated by NFIA and NFIB. Hence, specifically within the developing brain, NFIA and NFIB may share a conserved biological function.

In this study, we investigated whether NFIA and NFIB regulate similar biological processes during early cerebral development, as suggested by the overlapping phenotypes observed in mouse models and human patients. This would imply that within this context, NFIA and NFIB could function, at least in part, additively, and that the total 'gene dosage' of both factors could be important for normal cortical development. From these lines of evidence, we hypothesised that combined knockout of one allele of both *Nfia* and *Nfib* would result in a similar phenotype to the biallelic knockout of either family member, whereas knockout of more alleles of these genes would exacerbate the dysregulation of cellular differentiation and the observed brain developmental phenotype.

Materials and methods

Animal breeding

All breeding and experiments were performed at the State University of Buffalo under approval from the Institutional Animal Care and Use Committee, or at the University of Queensland in accordance with the Australian Code of Practice for the Care and Use of Animals for Scientific Purposes and with approval from the University of Queensland Animal Ethics Committee. *Nfia* knockout (*Nfia*^{tm1Rmg}) (Das Neves et al., 1999), *Nfib* knockout (*Nfib*^{tm1Rmg}) (Steele-Perkins et al., 2005), *Nfib*^{cond} conditional knockout (*Nfib*^{tm2Rmg}) (Hsu et al., 2011) and *R26-CreERT2* (*Gt(ROSA)26*$^{Sortm1(Cre/ERT2)Tyj}$) (Ventura et al., 2007) mice were maintained on a C57Bl/6 background. Individual alleles were genotyped as described previously (Das Neves et al., 1999; Harris et al., 2016; Hsu et al., 2011; Steele-Perkins et al., 2005).

To generate timed-pregnant females, male and female mice were placed together overnight, and the females checked the following day for vaginal plugs. This day was designated as embryonic day (E)0 if a vaginal plug was present. To induce deletion of the *Nfib*^{cond} allele in *Nfia;Nfib*^{cond}*;Rosa26-CreERT* mice, 2 mg tamoxifen (T-5648; Sigma) in corn oil was administered by intraperitoneal injection into dams at E10.5, E11.5 and E12.5 to generate double heterozygous (*Nfia*$^{+/-}$;*Nfib*$^{+/-}$) and homozygous (*Nfia*$^{-/-}$;*Nfib*$^{-/-}$) knockout embryos. Dams were euthanised using sodium pentobarbital (Abbott Laboratories), and embryos were drop fixed (E14 and below) or transcardially perfused with 0.9% (w/w) saline, followed by 4% paraformaldehyde in phosphate-buffered saline (PBS; pH 7.4) for further immunohistochemical analyses. For co-immunoprecipitation and RNA isolation, neocortical tissue was microdissected in ice-cold PBS. Samples used for RNA isolation were immediately snap frozen on dry ice, whereas co-immunoprecipitation was performed with fresh tissue samples. Frozen tissue was stored at −80°C until RNA isolation (Bunt et al., 2015).

RNA sequencing and analysis

Total RNA was isolated from frozen neocortical tissue using TRIzol Reagent as per the manufacturer's protocol (Life Technologies). Isolated RNA was treated with DNase (DNA-free DNA removal kit; Life Technologies). Libraries were prepared for 2 wildtype and 4 knockout *Nfia*$^{-/-}$ and 2 wildtype and 4 knockout *Nfib*$^{-/-}$ samples using the TruSeq RNA Library Preparation Kit v3 (paired-end 100nt length) and sequenced on an Illumina HiSeq 2000 (Illumina).

For analysis, paired-end reads from each sample were aligned to the mm9 reference genome using the TopHat2 algorithm version 2.0.10 (Kim et al., 2013). The change in expression in the *Nfia* and *Nfib* knockout tissue was calculated using gene expression levels in four *Nfia* and four *Nfib* knockout samples and their respective wildtype littermate samples (GSE93604). The fold change in expression and statistical significance were calculated using the CuffDiff tool version 2.1.1 (Trapnell et al., 2010).

Genes were considered regulated if the ^{2}log fold change of expression was >0.4 and the q-value was <0.05. Gene ontology analyses were performed using the DAVID tool (Huang da et al., 2009a, 2009b). To predict the presence of NFI binding motifs, we used the Find Individual Motif Occurrences tool (FIMO; Grant et al., 2011) with default programme significance threshold and the NFI motifs defined by Jolma et al. (2013). Enrichment of NFIB binding peaks (Chang et al., 2013; Lajoie et al., 2014) in the promoter were analysed as described previously (Bunt et al., 2012) and significance was determined by a chi-square test with Yates' corrections.

Real-time quantitative polymerase chain reaction analyses

Reverse transcription and real-time quantitative polymerase chain reaction (qPCR) analyses were performed on messenger RNA (mRNA) isolated from E16 *Nfia*$^{-/-}$, *Nfib*$^{-/-}$ or wildtype littermates as described previously (Lim et al., 2015). The thermocycler conditions used were as follows: 2 min at 50°C and 10 min at 95°C, followed by 45 cycles with 10 s denaturation at 95°C, 15 s annealing at 60°C and 20 s extension at 72°C. Relative expression was determined using the ΔΔCt method with *Hprt* as a reference gene. Statistical significance was determined using

two-tailed Student's t-tests. The primer sequences were as follows: *Alcam*, 5′-GGCAGTGGGAGCGTCATAAAC-3′ and 5′-ATCGCAGAGACATTCAGGGAG-3′; *Hprt*, 5′-GCAGTAC AGCCCCAAAATGG-3′ and 5′-AACAAAGTCTGGCCT GTATCCAA-3′; *Id4*, 5′-CAGTGCGATATGAACGACTGC-3′ and 5′-GACTTTCTTGTTGGGCGGGAT-3′; *Igfbp3*, 5′-CCA GGAAACATCAGTGAGTCC-3′ and 5′-GGATGGAACTTGGA ATCGGTCA-3′; *Mycn*, 5′-AACAACAAGGCGGTAACCAC-3′ and 5′-GAGGGTGCAGCATAGTTGTG-3′; *Pou3f1*, 5′-TCGA GGTGGGTGTCAAAGG-3′ and 5′-GGCGCATAAACGT CGTCCA-3′; *Tle4*, 5′-TTTACAGGCTCAATACCACAGTC-3′ and 5′-TGCACAGATAGCATTTAGTCGTT-3′.

Co-immunoprecipitation

Cytoplasmic and nuclear lysates were prepared from dissected neocortical tissue from E13 C57Bl/6J wildtype embryos as described previously (Klenova et al., 2002). A volume of 5 µg of co-immunoprecipitation antibody was pre-incubated with 15 µL Pierce Protein G magnetic beads (Thermo Scientific) in Tris-buffered saline containing 0.05% Tween-20 (v/v) (TBS.T; pH 7.5) for 4 h at 4°C prior to co-immunoprecipitation. Antibodies used for co-immunoprecipitation were rabbit anti-NFIA (HPA008884; Sigma), rabbit anti-NFIB (HPA003956; Sigma) and normal rabbit IgG (2729; Cell Signaling Technology). Antibody-bound beads were washed with TBS.T and co-immunoprecipitation buffer, and then incubated with nuclear lysate for 16 h at 4°C. Following co-immunoprecipitation, antibody-bound beads were washed thrice with co-immunoprecipitation buffer and prepared for Western blotting with NuPAGE LDS Sample Buffer (Invitrogen) and 0.1 M DL-dithiothreitol (Sigma). Samples were denatured by heating to 85°C for 10 min and electrophoresed on NuPAGE Novex 4%–12% Bis-Tris gels (Invitrogen). Electrophoresed samples were transferred to an Immobilon-FL polyvinylidene difluoride (PVDF) membrane (Merck Millipore) using the XCell II Blot Module (Invitrogen) according to the manufacturer's recommendations. Blotted membranes were blocked with 5% (w/v) skim milk powder in PBS and incubated with the appropriate primary antibody diluted with 5% (w/v) skim milk powder in PBS containing 0.1% (v/v) Tween-20 (PBS.T). The primary antibodies used for Western blots were rabbit anti-NFIA (1:1000, 39,397; Active Motif) and mouse anti-NFIB (1:100, ab51352; Abcam). The secondary antibodies used were IRDye 680LT donkey anti-rabbit and IRDye 800CW donkey anti-mouse (both diluted 1:15,000; LI-COR) diluted in PBS.T. Membranes were imaged using the Odyssey Classic (LI-COR) and Image Studio 5 software (LI-COR).

Immunohistochemistry and immunofluorescence

Dissected and post-fixed brains were embedded in 3% noble agar (Difco Sparks), and 50 µm coronal sections were cut using a vibratome (Lecia). Free-floating staining was performed as described previously (Barry et al., 2008; Campbell et al., 2008). The primary antibodies used for immunohistochemistry were rabbit anti-GFAP (1:30,000, Z0334; Dako), mouse anti-GAP43 monoclonal antibody (1:50,000, MAB1987; Millipore) and rabbit anti-TBR1 polyclonal antibody (1:1000, sc48816; Santa Cruz Biotechnology). A biotinylated goat anti-rabbit or anti-mouse secondary antibody (1:500; Jackson ImmunoResearch) was used, followed by incubation with the VECTASTAIN elite ABC kit (Vector Laboratories) and 3,3′-diaminobenzidine (DAB) staining as previously described (Plachez et al., 2008). Immunofluorescence co-staining on mounted sections was performed as described previously (Plachez et al., 2008). Sections were incubated with rabbit anti-NFIA (1:500, HPA008884; Sigma), rabbit anti-NFIB (1:500, HPA003956; Sigma), chicken anti-ß-galactosidase (1:500, ab9361; Abcam), rabbit anti-TBR1 polyclonal antibody (1:1000, sc48816; Santa Cruz Biotechnology), rat anti-CTIP2 (1:500, ab18465; Abcam), mouse anti-NeuN (1:1000, MAB377; Chemicon) followed by donkey Alexa Fluor 488, 555 or biotinylated labelled secondary antibodies (Invitrogen) and Alexa Fluor 647-conjugated Streptavidin (Invitrogen) amplification . Cell nuclei were stained using haematoxylin (Sigma) or 4′,6-diamidino-2-phenylindole (DAPI; Invitrogen). For all genotypes, matching sections of a minimum of six animals were analysed, except for *Nfia*;*Nfib* double homozygous knockout mice, for which three embryos were analysed due to the reduced viability of these embryos.

Imaging and analyses

Brightfield imaging was performed with a Zeiss upright AxioImager Z1 microscope fitted with Axio-Cam HRc and HRm cameras. Images were acquired with the ZEN blue software (Carl Zeiss). Immunofluorescence images were obtained from a Diskovery inverted spinning-disk confocal system (Spectral Applied Research) consisting of a Ti-E microscope (Nikon) equipped with a Diskovery disk head (Spectral Applied Research), two Flash4.0 sCMOS cameras (Hamamatsu Photonics) and 20× 0.75 NA CFI PlanApo and 40× 1.15 NA CFI ApoLambda objectives. Images were pseudo-coloured to permit overlay and were then cropped, sized and contrast-brightness enhanced for presentation with Photoshop software (Adobe). For quantification, cortical measurements were taken from haematoxylin-stained matched sections of three to five animals per condition. All measurements were averaged from both hemispheres of each animal. Statistical significance was determined using two-tailed Student's t-test.

Results

Radial glia co-express NFIA and NFIB during development

The individual expression of NFIA and NFIB has been reported in radial glia from E12 in mice (Betancourt et al., 2014; Bunt et al., 2015; Plachez et al., 2008), but their co-expression within these cells has not been determined. To exclude the possibility that knockout of *Nfia* and *Nfib* affected different subpopulations of radial glia, we analysed their co-expression at a cellular level in the developing cerebrum. The *Nfib* locus carries a knock-in β-*galactosidase* reporter gene substituted into the deleted exon of the *Nfib* allele as a marker for NFIB expression (Betancourt et al., 2014; Piper et al., 2009; Steele-Perkins et al., 2005). For each stage examined, we validated β-galactosidase and NFIB co-expression (Figure 1) to ensure that we were able to analyse co-expression of NFIA and NFIB using β-galactosidase protein expression as a reporter with fidelity (Figure 2). At E13, both NFIA and

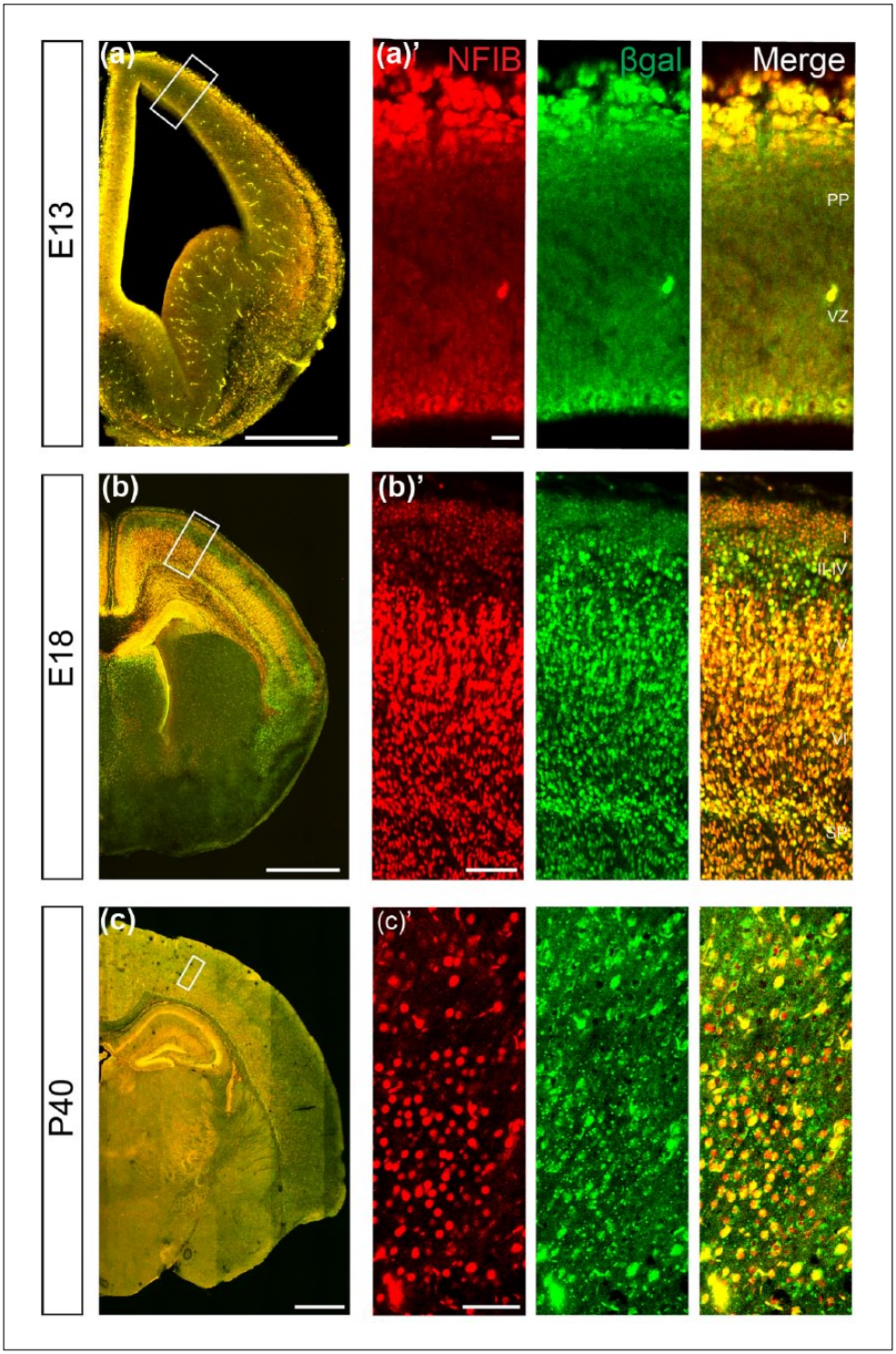

Figure 1. NFIB and β-galactosidase reporter proteins are co-expressed during cortical development.
The expression of β-galactosidase (βgal) and NFIB proteins overlap in heterozygous *Nfib* knockout mice. The β-galactosidase gene is knocked into exon 2 of the deleted *Nfib* allele. Thus, this marker protein acts as a reporter for NFIB expression (Betancourt et al., 2014; Piper et al., 2009; Steele-Perkins et al., 2005). At E13 (a), E18 (b) and P40 (c) both proteins were co-expressed throughout the cerebrum.
Scale bar: a–c = 300 μm; a′, c′ = 20 μm; b′ = 100 μm. PP: preplate; VZ: ventricular zone; I–VI: cortical layers; SP: subplate.

β-galactosidase were co-expressed in a high medial to low lateral gradient in the coronal plane throughout the ventricular zone (VZ) of the cerebral cortex. At later stages of development, such as E18, the VZ of the cerebral cortex and hippocampus still co-expressed both proteins, but their expression had started to diverge in the post-mitotic progeny (Figure 2(b)–(e) and Figure 3). While NFIA

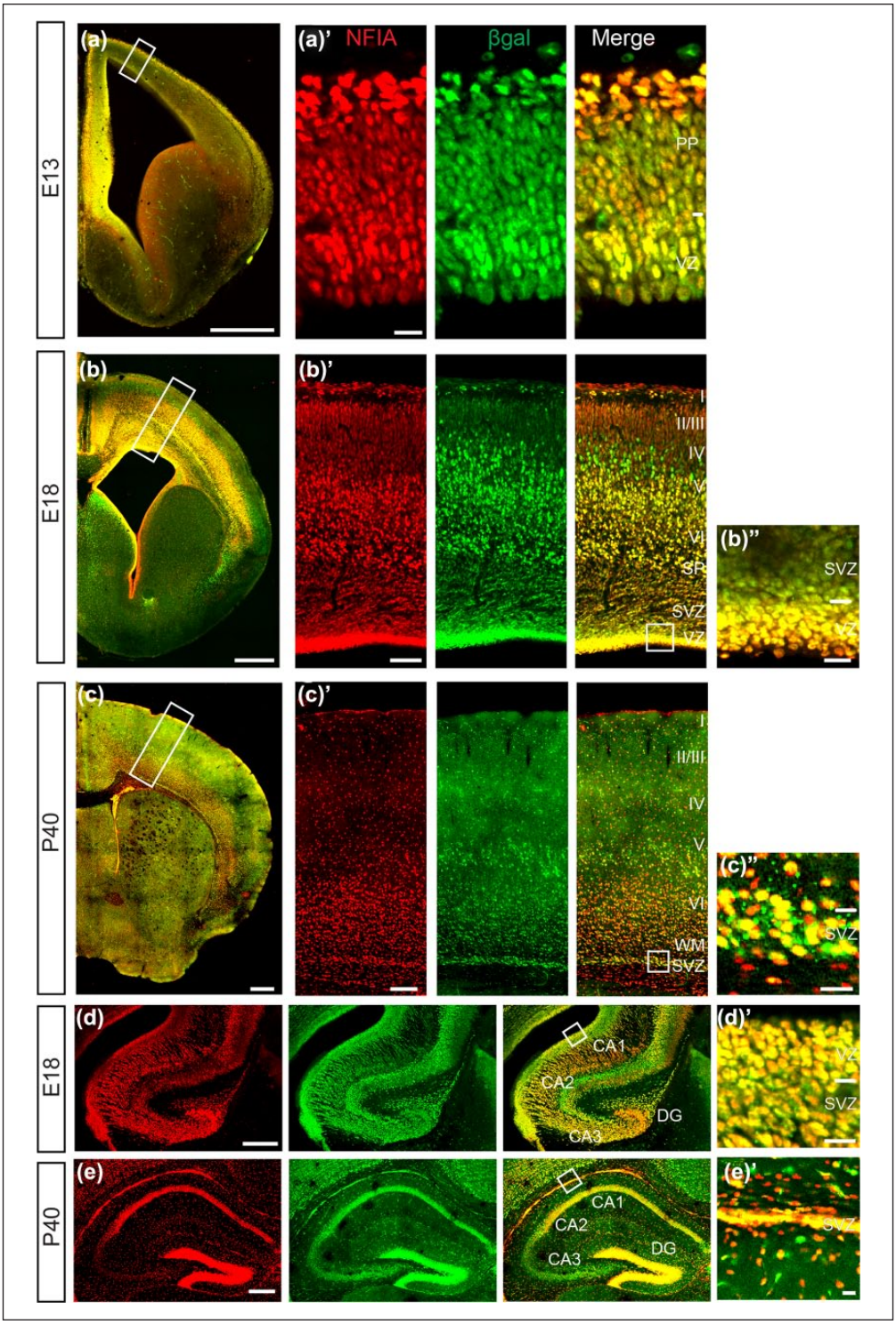

Figure 2. NFIA and NFIB are co-expressed in radial glia during cortical development.

Co-expression of NFIA and NFIB was analysed by immunofluorescent labelling of NFIA and β-galactosidase (βgal) reporter protein in *Nfib*$^{+/-}$ knockout mice. The β-*galactosidase* gene was knocked into exon 2 of the deleted *Nfib* allele and thereby recapitulates NFIB expression (Betancourt et al., 2014; Piper et al., 2009; Steele-Perkins et al., 2005). At E13 (a) and E18 (b), both proteins were co-expressed throughout the cerebrum in a high medial to low lateral gradient. This included high expression in the radial glia in the ventricular zone (a′ and b′). In the cortical plate, there was less overlap in NFIA and NFIB expression (b′, c and c′). Ependymal cells, representing terminally differentiated radial glia, retained high co-expression of both proteins (c″). Similarly, in the developing hippocampus (d), NFIA and NFIB were co-expressed in the proliferative zone (d′), whereas expression was more variable in the other cell types. Postnatally, NFIA and NFIB remained co-expressed in the ependymal cells and neural progenitors of the dentate gyrus (e and e′).

Scale bar: a–c = 300 μm; b′, c′, d, e = 100 μm; a′, b″, c″, d′, e′ = 20 μm. PP: preplate; VZ: ventricular zone; I–VI: cortical layers; SP: subplate; SVZ: subventricular zone; WM: white matter; DG: dentate gyrus; CA1–3: hippocampal subfields.

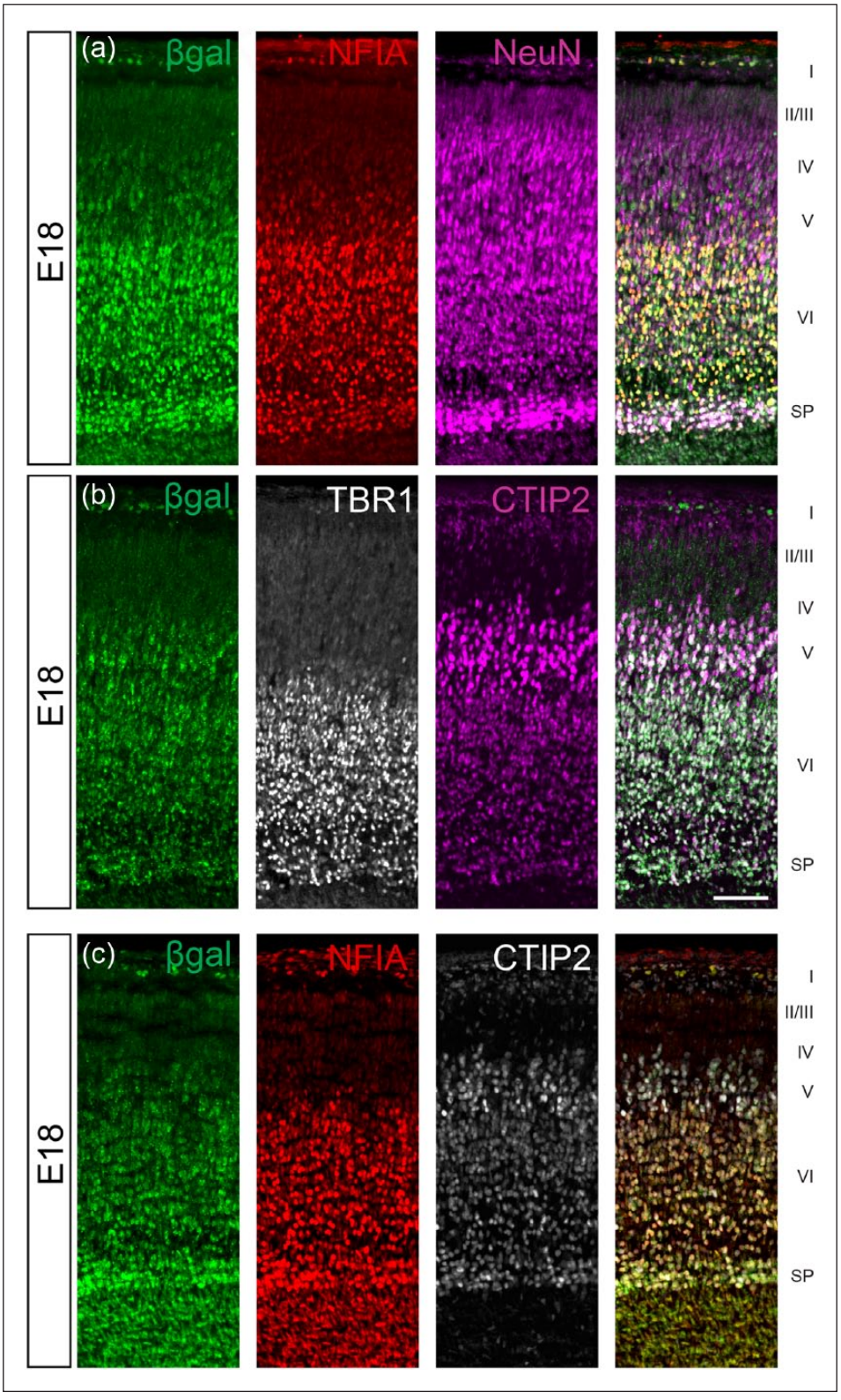

Figure 3. NFIA and β-galactosidase reporter protein expression in the cortical layers during late cortical development.
At E18, β-galactosidase (βgal) and NFIA proteins are co-expressed in the neurons of the subplate and layer VI of the cortical plate as assessed by expression of NeuN (a). However, β-galactosidase expression extents further as shown by co-expression with layer V marker CTIP2 and layer VI marker TBR1 (b). In contrast, little co-expression of NFIA with CTIP2 was detected (c). Hence, the E18 cortical plate already resembles the layer specific expression as detected in the adult mouse brain (Chen et al., 2017).
Scale bar = 100 μm. I, II/III, IV, V, VI: cortical layers; SP: subplate.

and β-galactosidase were co-expressed in the subplate and layer VI of the neocortex, NFIB expression extended more dorsally than NFIA at E18 (Figures 2(b) and 3). Similarly, expression of β-galactosidase extends further into the hippocampal plate. Postnatally, NFIA and NFIB remained co-expressed in the neural progenitor cells of the dentate gyrus and by the ependymal cells lining the lateral ventricles (Figure 2(c) and (e)). In line with our previous work detailing expression of NFI proteins in the adult mouse brain (Chen et al., 2017), NFIA and NFIB remained highly co-expressed in the pyramidal layer and dentate gyrus in the hippocampus, while the expression of these factors within the neocortex was more diverse. Hence, deletion of *Nfia* and *Nfib* will likely affect the same population of radial glia.

NFIA and NFIB share regulation of downstream target genes involved in neurodevelopment

Although mRNA expression analyses of *Nfia* and *Nfib* knockout embryos have revealed several common downstream targets (Barry et al., 2008; Betancourt et al., 2014; Harris et al., 2016; Piper et al., 2009, 2010, 2014), the overlap of these factors in regulating downstream targets and pathways remained unclear. We therefore analysed mRNA-sequencing data from the cerebral cortex of E16 *Nfia* and *Nfib* knockout mice and their corresponding wildtype littermates. Using thresholds of ^{2}log fold change >0.4 and q-value <0.05, 540 and 738 genes were differentially regulated in *Nfia* and *Nfib* knockout mice, respectively. Of these, 91 genes showed similar misregulation in both *Nfia* and *Nfib* knockout mice, when we allowed for a less stringent q-value of <0.1 in one mouse model to compensate for experimental variability (Table 1). We validated the misregulation of the genes *Alcam*, *Id4*, *Igfbp3*, *Mycn*, *Pou3f1* and *Tle4* by qPCR (Table 2).

Functional annotation clustering using DAVID (Huang da et al., 2009a, 2009b) confirmed that the 91 shared genes were enriched for neurodevelopment-related gene ontology terms (Table 3; $p < 0.05$ with Benjamini–Hochberg correction). Similarly, when we performed gene ontology separately on the differentially regulated genes identified from only one mouse model (Table 4; 540 genes for *Nfia* and 738 genes for *Nfib*; $p < 0.005$ with Benjamini–Hochberg correction), the gene ontology terms that were common to both mouse models also consisted of neurodevelopment-related processes. In contrast, gene ontology terms unique to only one *Nfi* knockout model were also related to NFI function in other organs, such as lung development for NFIB (Steele-Perkins et al., 2005). Collectively, these results suggest that NFIA and NFIB are likely to co-regulate a core neurodevelopmental programme to drive embryonic corticogenesis.

Shared misregulated genes in Nfi knockout neocortex are enriched for NFI binding

To test whether the 91 shared misregulated genes are more likely to represent direct NFI targets, we determined whether predicted NFI binding motifs (Jolma et al., 2013) were present in their respective promoters. Although such a motif was present in 59.5% of all genes in the genome within 2000 base pairs of the transcription start sites, this value increased to 71.7% and 71.3% in the 540 and 738 differentially regulated genes identified in *Nfia* and *Nfib* knockout mice, respectively (Figure 4(a)). The 91 similarly misregulated genes showed even higher enrichment, with 85.7% having at least one predicted NFI binding motif.

Not all predicted binding motifs might represent true NFI binding sites. To assess whether NFIB could bind to the promoter of these differentially expressed genes, we analysed the presence of an NFIB binding peak in their promoter using published NFIB chromatin immunoprecipitation-sequencing (ChIP-sequencing) data reported in other tissues (Chang et al., 2013; Lajoie et al., 2014). The presence of an NFIB binding peak detected within a gene promoter from a ChIP-sequencing dataset from mouse hair follicle stem cells increased from 1.1% in the promoter of all genes to 1.5% and 2.7% in the differentially regulated genes that we identified in the *Nfia* and *Nfib* knockout mice, respectively (Figure 4(b)). Similarly, the presence of an NFIB binding peak detected within a ChIP-sequencing dataset from E16 lung tissue increased from 6.9% (all genes) to 10.2% (*Nfia* knockout) and 12.6% (*Nfib* knockout) (Figure 4(c)). The misregulated genes in our analysis were therefore more likely to contain a putative NFI binding site within their promoter.

The 91 misregulated genes shared between *Nfia* and *Nfib* showed even higher enrichment for putative NFI binding sites: 5.5% and 17.6% in hair follicle and lung datasets, respectively (Chang et al., 2013; Lajoie et al., 2014). NFIB binding peaks were more prevalent in the genes that were down-regulated following *Nfi* deletion (striped bars in Figure 4(b) and (c)), displaying enrichments of 8.1% (hair follicle) and 22.6% (lung). This enrichment increased to 9.8% and 34.1%, respectively, when we increased the minimal ^{2}log fold change to >0.6. Hence, NFI-activated genes that are down-regulated in both *Nfia* and *Nfib* knockout mice are more likely to represent direct targets of both NFIA and NFIB.

To identify shared targets that are expressed specifically within cortical radial glia, we utilised the differential expression modules described for the E14.5 neocortex by Fietz et al. (2012). Compared to all genes (8.1%), genes that were down-regulated in both *Nfia* and *Nfib* knockout mice were enriched for high expression in the VZ (23.1%, or 12 out of 52 shared down-regulated genes; Yates < .0001) (Tables 1 and 2). We were also able to verify the high VZ expression of these 12 genes using in situ hybridisation datasets (Tables 1 and 2) (Allen Institute, 2013; Diez-Roux et al., 2011; Kawaguchi et al., 2008; Shimogori et al., 2010; Visel et al., 2004). Furthermore, 7 out of the 12 down-regulated genes showed NFIB binding in their promoter in either lung or hair follicle ChIP-sequencing datasets, while only 9 out of the remaining 40 down-regulated genes had binding. Hence, these seven genes, *Bcan*, *Kcne1l*, *Loxl1*, *Ltbp1*, *Mfge8*, *Slc9a3r1* and *Tnc*, are likely to be directly regulated by NFIA and NFIB in radial glia, and may be responsible for the similar cortical developmental defects that are observed in single knockout mice.

NFIA and NFIB dimerise in vivo

Besides recognising the same DNA motif (Jolma et al., 2013), NFIA and NFIB could physically interact with each other through protein dimerisation. The NFI DNA binding motif consists of two palindromic recognition sites, and *in vitro* analysis has demonstrated the binding of two NFI proteins at such sites (Gronostajski et al., 1985; Leegwater et al., 1985). Furthermore, both hetero- and homodimers have been

Table 1. Common misregulated genes in *Nfia* and *Nfib* knockout E16 neocortical tissue.

Gene	Nfia knockout		Nfib knockout		NFI motif	NFIB peak (hair)	NFIB peak (lung)	VZ high module (Fietz et al.)	VZ expression validation	High caudal – low rostral gradient
	^{2}log fold change	q-value	^{2}log fold change	q-value						
Acvr1c	−0.66	6.32E−02	−1.945	2.07E−03	Promoter	#N/A	#N/A			
Adcyap1	−0.66	6.47E−02	−0.953	2.07E−03	Promoter	#N/A	#N/A			
Aox4	−1.78	2.86E−03	−2.310	2.07E−03	Promoter	Promoter	#N/A			
Arhgap28	−0.98	2.86E−03	−1.672	2.07E−03	#N/A	#N/A	#N/A			
Bcan	−0.93	2.86E−03	−2.723	2.07E−03	Promoter	#N/A	Promoter	Y	Y	Y
Cbs	−1.35	2.86E−03	−1.669	2.07E−03	Promoter	#N/A	#N/A	Y	Y	?
Ccdc80	−0.79	5.05E−03	−0.688	1.06E−02	Promoter	#N/A	#N/A	Y	Y	Y
Clstn2	−0.64	2.86E−03	−0.516	1.30E−02	Promoter	#N/A	#N/A			
Cnih3	−0.44	5.80E−02	−0.748	2.07E−03	Promoter	#N/A	#N/A			
Cnr1	−0.48	1.79E−02	−0.824	2.07E−03	Promoter	#N/A	#N/A			
Col12a1	−0.96	2.86E−03	−1.592	2.07E−03	Promoter	#N/A	#N/A	Y	Y	?
Col15a1	−0.78	2.86E−03	−1.044	2.07E−03	Promoter	#N/A	#N/A			
Crtc3	−0.53	2.58E−02	−0.686	5.32E−03	Promoter	#N/A	#N/A			
Dhrs3	−1.28	2.86E−03	−2.306	2.07E−03	Promoter	Promoter	Promoter	Y	Y	?
Dio2	−1.91	2.86E−03	−3.163	2.07E−03	Promoter	#N/A	#N/A			
Dok5	−0.61	2.86E−03	−1.069	2.07E−03	Promoter	#N/A	Promoter			
Dync1i1	−0.52	1.21E−02	−0.651	2.07E−03	Promoter	#N/A	#N/A			
Ermn	−1.00	1.94E−02	−1.610	2.07E−03	Promoter	#N/A	Promoter			
Fam174b	−0.48	5.18E−02	−0.625	1.19E−02	Promoter	#N/A	#N/A			
Frmd6	−0.56	3.58E−02	−0.921	2.07E−03	#N/A	#N/A	#N/A			
Gdf5	−0.98	8.81E−02	−2.057	2.07E−03	Promoter	#N/A	#N/A			
Gipr	−0.68	2.86E−03	−0.563	4.24E−02	Promoter	#N/A	#N/A			
Glt28d2	−1.22	6.89E−03	−0.951	8.93E−02	Promoter	#N/A	#N/A			
Gucy1a3	−0.62	2.86E−03	−1.569	2.07E−03	Promoter	#N/A	#N/A			
Hspb3	−1.32	9.54E−02	−2.234	1.30E−02	Promoter	#N/A	Promoter			
Htr3a	−1.05	1.63E−02	−3.541	2.07E−03	Promoter	#N/A	Promoter			
Igfbp3*	−0.64	2.86E−03	−1.600	2.07E−03	#N/A	#N/A	#N/A			
Itpr1	−0.65	2.86E−03	−0.485	1.62E−02	Promoter	#N/A	#N/A			
Jakmip3	−0.73	2.86E−03	−1.744	2.07E−03	Promoter	#N/A	#N/A			
Kcne1l	−1.05	6.89E−03	−1.485	2.07E−03	Promoter	#N/A	#N/A	Y	Y	?
Kcnj2	−0.78	2.86E−03	−0.981	2.07E−03	Promoter	#N/A	Promoter			
Kcnq5	−0.56	1.04E−02	−0.807	2.07E−03	#N/A	#N/A	#N/A			
Lhx2	−0.65	2.86E−03	−0.459	3.57E−02	Promoter	Promoter	#N/A			
Lifr	−0.52	6.47E−02	−0.792	6.76E−03	Promoter	#N/A	#N/A			
Lmo7	−0.66	2.86E−03	−1.165	2.07E−03	Promoter	#N/A	#N/A			
Loxl1	−3.43	2.86E−03	−2.699	2.07E−03	Promoter	#N/A	Promoter	Y	Y	?
Ltbp1	−0.97	2.86E−03	−1.636	2.07E−03	Promoter	#N/A	Promoter	Y	Y	?
March4	−0.49	1.34E−02	−0.808	2.07E−03	Promoter	#N/A	#N/A			
Mfge8	−0.86	2.86E−03	−1.381	2.07E−03	Promoter	Promoter	#N/A	Y	Y	N
Mycn*	−0.48	8.59E−03	−0.550	9.42E−03	#N/A	#N/A	#N/A			
Npr3	−1.17	2.86E−03	−2.156	2.07E−03	Promoter	#N/A	#N/A			
Nr4a3	−0.66	1.63E−02	−2.160	2.07E−03	Promoter	#N/A	#N/A			
Nrp1	−0.68	2.86E−03	−0.726	2.07E−03	Promoter	#N/A	Promoter			
Ntrk3	−0.49	3.09E−02	−0.576	9.42E−03	#N/A	#N/A	#N/A			
Olfml2b	−0.72	1.48E−02	−0.654	3.86E−02	Promoter	#N/A	Promoter			
Palmd	−0.85	2.86E−03	−0.816	2.07E−03	#N/A	Promoter	Promoter			
Pdzrn3	−0.49	2.58E−02	−0.617	5.32E−03	Promoter	#N/A	#N/A			
Pou3f1*	−0.59	6.89E−03	−0.692	2.07E−03	Promoter	#N/A	#N/A			
Rnf182	−0.44	4.58E−02	−0.483	3.08E−02	Promoter	#N/A	#N/A			
Rspo3	−0.67	2.86E−03	−0.573	6.52E−02	Promoter	#N/A	#N/A			
Slc14a2	−0.99	5.18E−02	−1.208	1.81E−02	Promoter	#N/A	#N/A			

(Continued)

Table 1. (Continued)

Gene	Nfia knockout		Nfib knockout		NFI motif	NFIB peak (hair)	NFIB peak (lung)	VZ high module (Fietz et al.)	VZ expression validation	High caudal – low rostral gradient
	^{2}log fold change	q-value	^{2}log fold change	q-value						
Slc26a7	–1.37	6.89E–03	–3.220	2.07E–03	Promoter	#N/A	#N/A	Y	Y	Y
Slc7a2	–0.66	2.58E–02	–0.719	2.01E–02	Promoter	#N/A	#N/A			
Slc9a3r1	–0.77	6.89E–03	–0.994	2.07E–03	Promoter	#N/A	Promoter	Y	Y	Y
Slco1c1	–0.61	3.80E–02	–1.446	2.07E–03	Promoter	#N/A	#N/A			
Stac2	–0.88	2.86E–03	–1.388	2.07E–03	Promoter	#N/A	#N/A			
Tcerg1l	–0.87	2.86E–03	–2.892	2.07E–03	Promoter	#N/A	#N/A			
Tenm2	–0.51	2.86E–03	–1.310	2.07E–03	Promoter	#N/A	#N/A			
Tle4*	–0.59	2.86E–03	–0.606	2.07E–03	Promoter	#N/A	#N/A			
Tnc	–1.14	2.86E–03	–1.718	2.07E–03	Promoter	#N/A	Promoter	Y	Y	?
Trim47	–1.48	1.63E–02	–1.667	2.07E–03	Promoter	#N/A	#N/A			
Whrn	–0.71	2.86E–03	–0.923	2.07E–03	#N/A	#N/A	#N/A			
6330403A02Rik	0.58	2.86E–03	0.916	2.07E–03	Promoter	#N/A	Promoter			
Alcam*	0.44	2.58E–02	1.055	2.07E–03	Promoter	#N/A	#N/A			
Amot	0.44	6.24E–02	0.806	2.07E–03	Promoter	#N/A	#N/A			
Apcdd1	0.50	1.34E–02	0.925	2.07E–03	Promoter	#N/A	#N/A			
Arhgef28	0.52	2.35E–02	0.853	2.07E–03	Promoter	#N/A	#N/A			
Btbd3	0.64	2.86E–03	0.535	1.30E–02	Promoter	#N/A	#N/A			
Cdhr1	1.36	2.86E–03	0.973	2.50E–02	Promoter	#N/A	#N/A			
Chrm2	1.05	1.34E–02	1.137	2.80E–02	Promoter	#N/A	#N/A			
Col14a1	0.87	4.40E–02	1.303	3.85E–03	Promoter	#N/A	#N/A			
Dner	0.69	2.86E–03	0.576	3.85E–03	Promoter	#N/A	#N/A			
Fam184b	0.84	8.59E–03	0.801	1.81E–02	Promoter	#N/A	#N/A			
Fbn1	0.62	2.86E–03	0.740	2.07E–03	#N/A	#N/A	#N/A			
Fstl5	0.43	4.76E–02	0.417	8.90E–02	#N/A	#N/A	#N/A			
Grin3a	0.90	2.86E–03	0.468	6.63E–02	Promoter	#N/A	Promoter			
Id4*	0.42	9.03E–02	0.866	2.07E–03	Promoter	#N/A	#N/A			
Kcnk12	1.12	2.09E–02	1.102	7.44E–02	#N/A	#N/A	#N/A			
Lhfpl3	0.95	2.86E–03	0.628	4.42E–02	#N/A	#N/A	#N/A			
Lrrtm3	0.56	6.89E–03	0.612	1.06E–02	Promoter	#N/A	#N/A			
Ndst4	1.32	2.86E–03	1.094	3.32E–02	Promoter	#N/A	#N/A			
Pid1	0.80	2.86E–03	0.655	2.07E–03	Promoter	#N/A	#N/A			
Prkg2	1.16	4.12E–02	1.153	4.49E–02	Promoter	#N/A	#N/A			
Slc17a7	0.44	4.19E–02	0.569	5.32E–03	Promoter	#N/A	#N/A			
Slc24a2	0.97	2.86E–03	1.121	2.07E–03	Promoter	#N/A	#N/A			
Slc44a5	0.51	4.58E–02	0.901	2.07E–03	Promoter	#N/A	#N/A			
Stat4	1.40	4.30E–02	2.187	2.07E–03	Promoter	#N/A	#N/A			
Trpc5	0.86	6.89E–03	0.735	9.31E–02	#N/A	#N/A	#N/A			
Ttc7	0.88	2.86E–03	1.811	2.07E–03	Promoter	#N/A	#N/A			
Ttr	1.71	1.34E–02	8.104	2.07E–03	Promoter	#N/A	#N/A			
Unc13c	1.01	2.86E–03	0.982	2.07E–03	Promoter	#N/A	#N/A			

*qPCR validated.

Table 2. qPCR validation of six selected misregulated genes in *Nfia* and *Nfib* knockout.

Gene	Nfia knockout		Nfib knockout	
	^{2}log fold change again	p-value	^{2}log fold change	p-value
Igfbp3	–0.47	8.83E–04	–0.63	7.37E–04
Mycn	–0.38	5.05E–02	–0.41	8.36E–03
Pou3f1	–0.27	1.59E–04	–0.37	3.15E–04
Tle4	–0.40	2.64E–02	–0.38	1.88E–02
Alcam	0.33	2.31E–03	0.60	4.26E–03
Id4	0.53	2.64E–02	0.81	1.88E–02

Table 3. Gene ontology enrichment of 91 common misregulated genes in *Nfia* and *Nfib* knockout E16 neocortical tissue.

Category	Term	Benjamini-corrected p-value
GOTERM_BP_FAT	GO:0007399~nervous system development	1.41E–03
GOTERM_BP_FAT	GO:0022008~neurogenesis	6.27E–03
GOTERM_BP_FAT	GO:0030182~neuron differentiation	1.80E–02
GOTERM_BP_FAT	GO:0042391~regulation of membrane potential	2.72E–02
GOTERM_BP_FAT	GO:0048666~neuron development	3.27E–02
GOTERM_BP_FAT	GO:0007417~central nervous system development	2.88E–02
GOTERM_BP_FAT	GO:0048468~cell development	2.76E–02
GOTERM_BP_FAT	GO:0048699~generation of neurons	2.54E–02
GOTERM_BP_FAT	GO:0048667~cell morphogenesis involved in neuron differentiation	2.66E–02
GOTERM_BP_FAT	GO:0007267~cell-cell signalling	3.13E–02
GOTERM_BP_FAT	GO:0061564~axon development	3.50E–02
GOTERM_BP_FAT	GO:0031175~neuron projection development	3.37E–02
GOTERM_BP_FAT	GO:0006811~ion transport	4.03E–02
GOTERM_BP_FAT	GO:0023051~regulation of signalling	4.66E–02

Table 4. Gene ontology enrichment for biological processes of regulated targets in *Nfi* knockout E16 cortex.

Category	Term	Benjamini-corrected p-value	
		Nfia knockout	Nfib knockout
GOTERM_BP_FAT	GO:0050801~ion homeostasis	2.17E–02	
GOTERM_BP_FAT	GO:0006812~cation transport	8.20E–06	
GOTERM_BP_FAT	GO:0006813~potassium ion transport	4.62E–05	
GOTERM_BP_FAT	GO:0006816~calcium ion transport	1.86E–03	
GOTERM_BP_FAT	GO:0007156~homophilic cell adhesion	3.49E–02	
GOTERM_BP_FAT	GO:0010769~regulation of cell morphogenesis involved in differentiation	1.53E–02	
GOTERM_BP_FAT	GO:0015672~monovalent inorganic cation transport	2.26E–04	
GOTERM_BP_FAT	GO:0015674~di-, tri-valent inorganic cation transport	1.60E–02	
GOTERM_BP_FAT	GO:0042471~ear morphogenesis	2.98E–02	
GOTERM_BP_FAT	GO:0042472~inner ear morphogenesis	1.66E–02	
GOTERM_BP_FAT	GO:0046928~regulation of neurotransmitter secretion	8.51E–03	
GOTERM_BP_FAT	GO:0048562~embryonic organ morphogenesis	3.77E–02	
GOTERM_BP_FAT	GO:0048839~inner ear development	1.95E–02	
GOTERM_BP_FAT	GO:0050770~regulation of axonogenesis	2.02E–02	
GOTERM_BP_FAT	GO:0051588~regulation of neurotransmitter transport	1.20E–02	
GOTERM_BP_FAT	GO:0000902~cell morphogenesis	4.49E–02	3.76E–11
GOTERM_BP_FAT	GO:0000904~cell morphogenesis involved in differentiation	9.41E–03	4.15E–12
GOTERM_BP_FAT	GO:0001764~neuron migration	2.02E–02	7.88E–04
GOTERM_BP_FAT	GO:0006811~ion transport	3.11E–07	1.72E–02
GOTERM_BP_FAT	GO:0006873~cellular ion homeostasis	2.13E–02	2.51E–02
GOTERM_BP_FAT	GO:0006928~cell motion	3.63E–03	9.40E–09
GOTERM_BP_FAT	GO:0007155~cell adhesion	4.05E–06	9.32E–05
GOTERM_BP_FAT	GO:0007167~enzyme linked receptor protein signalling pathway	7.42E–03	1.11E–03
GOTERM_BP_FAT	GO:0007267~cell-cell signalling	5.74E–07	6.87E–08
GOTERM_BP_FAT	GO:0007268~synaptic transmission	4.35E–05	9.81E–04
GOTERM_BP_FAT	GO:0007409~axonogenesis	1.66E–02	3.83E–13
GOTERM_BP_FAT	GO:0007411~axon guidance	4.38E–03	6.64E–12
GOTERM_BP_FAT	GO:0007423~sensory organ development	4.21E–02	2.52E–03
GOTERM_BP_FAT	GO:0007610~behaviour	2.63E–03	1.91E–03
GOTERM_BP_FAT	GO:0010975~regulation of neuron projection development	2.55E–03	3.86E–02
GOTERM_BP_FAT	GO:0016477~cell migration	5.11E–03	3.99E–04
GOTERM_BP_FAT	GO:0019226~transmission of nerve impulse	3.22E–05	1.53E–04
GOTERM_BP_FAT	GO:0022604~regulation of cell morphogenesis	9.86E–04	2.91E–04

Table 4. (Continued)

Category	Term	Benjamini-corrected p-value	
		Nfia knockout	Nfib knockout
GOTERM_BP_FAT	GO:0022610~biological adhesion	3.37E–06	9.47E–05
GOTERM_BP_FAT	GO:0030001~metal ion transport	9.56E–07	2.10E–02
GOTERM_BP_FAT	GO:0030030~cell projection organisation	7.47E–03	1.05E–10
GOTERM_BP_FAT	GO:0030182~neuron differentiation	4.05E–05	2.55E–13
GOTERM_BP_FAT	GO:0030534~adult behaviour	9.44E–03	2.49E–03
GOTERM_BP_FAT	GO:0030900~forebrain development	2.04E–02	1.20E–09
GOTERM_BP_FAT	GO:0031175~neuron projection development	5.26E–03	5.95E–12
GOTERM_BP_FAT	GO:0031344~regulation of cell projection organisation	2.62E–04	2.94E–02
GOTERM_BP_FAT	GO:0032990~cell part morphogenesis	1.98E–02	1.04E–11
GOTERM_BP_FAT	GO:0033555~multicellular organismal response to stress	1.67E–02	1.26E–02
GOTERM_BP_FAT	GO:0044057~regulation of system process	7.38E–04	1.63E–03
GOTERM_BP_FAT	GO:0045664~regulation of neuron differentiation	5.51E–03	3.75E–05
GOTERM_BP_FAT	GO:0048666~neuron development	1.28E–04	2.55E–11
GOTERM_BP_FAT	GO:0048667~cell morphogenesis involved in neuron differentiation	6.62E–03	4.38E–12
GOTERM_BP_FAT	GO:0048812~neuron projection morphogenesis	1.22E–02	5.11E–13
GOTERM_BP_FAT	GO:0048858~cell projection morphogenesis	1.51E–02	3.98E–12
GOTERM_BP_FAT	GO:0048870~cell motility	1.07E–02	1.90E–03
GOTERM_BP_FAT	GO:0050767~regulation of neurogenesis	2.69E–02	7.01E–05
GOTERM_BP_FAT	GO:0051674~localisation of cell	1.07E–02	1.90E–03
GOTERM_BP_FAT	GO:0055082~cellular chemical homeostasis	2.73E–02	3.19E–02
GOTERM_BP_FAT	GO:0060284~regulation of cell development	3.53E–02	1.20E–06
GOTERM_BP_FAT	GO:0000122~negative regulation of transcription from RNA polymerase II promoter		1.56E–02
GOTERM_BP_FAT	GO:0001568~blood vessel development		2.99E–03
GOTERM_BP_FAT	GO:0001654~eye development		4.16E–03
GOTERM_BP_FAT	GO:0001708~cell fate specification		3.21E–03
GOTERM_BP_FAT	GO:0001944~vasculature development		1.80E–03
GOTERM_BP_FAT	GO:0003002~regionalisation		1.43E–03
GOTERM_BP_FAT	GO:0003013~circulatory system process		2.49E–02
GOTERM_BP_FAT	GO:0006357~regulation of transcription from RNA polymerase II promoter		9.11E–05
GOTERM_BP_FAT	GO:0007169~transmembrane receptor protein tyrosine kinase signalling pathway		2.56E–02
GOTERM_BP_FAT	GO:0007200~activation of phospholipase C activity by G-protein coupled receptor protein signalling pathway coupled to IP3 second messenger		4.43E–02
GOTERM_BP_FAT	GO:0007224~smoothened signalling pathway		1.55E–02
GOTERM_BP_FAT	GO:0007389~pattern specification process		1.31E–04
GOTERM_BP_FAT	GO:0007405~neuroblast proliferation		4.07E–02
GOTERM_BP_FAT	GO:0007507~heart development		4.64E–02
GOTERM_BP_FAT	GO:0007517~muscle organ development		2.63E–02
GOTERM_BP_FAT	GO:0007519~skeletal muscle tissue development		3.58E–03
GOTERM_BP_FAT	GO:0008015~blood circulation		2.49E–02
GOTERM_BP_FAT	GO:0008217~regulation of blood pressure		1.92E–02
GOTERM_BP_FAT	GO:0008284~positive regulation of cell proliferation		3.92E–03
GOTERM_BP_FAT	GO:0008285~negative regulation of cell proliferation		1.16E–02
GOTERM_BP_FAT	GO:0008360~regulation of cell shape		3.86E–02
GOTERM_BP_FAT	GO:0009890~negative regulation of biosynthetic process		1.73E–02
GOTERM_BP_FAT	GO:0009891~positive regulation of biosynthetic process		4.00E–03
GOTERM_BP_FAT	GO:0009953~dorsal/ventral pattern formation		1.77E–02
GOTERM_BP_FAT	GO:0009954~proximal/distal pattern formation		9.42E–03
GOTERM_BP_FAT	GO:0009968~negative regulation of signal transduction		4.67E–02
GOTERM_BP_FAT	GO:0010557~positive regulation of macromolecule biosynthetic process		3.31E–03
GOTERM_BP_FAT	GO:0010558~negative regulation of macromolecule biosynthetic process		1.86E–02
GOTERM_BP_FAT	GO:0010604~positive regulation of macromolecule metabolic process		1.13E–02
GOTERM_BP_FAT	GO:0010605~negative regulation of macromolecule metabolic process		2.49E–02
GOTERM_BP_FAT	GO:0010628~positive regulation of gene expression		3.56E–04

(Continued)

Table 4. (Continued)

Category	Term	Benjamini-corrected p-value	
		Nfia knockout	Nfib knockout
GOTERM_BP_FAT	GO:0010629~negative regulation of gene expression		8.51E–03
GOTERM_BP_FAT	GO:0010648~negative regulation of cell communication		1.96E–02
GOTERM_BP_FAT	GO:0014706~striated muscle tissue development		1.08E–02
GOTERM_BP_FAT	GO:0016055~Wnt receptor signalling pathway		4.96E–03
GOTERM_BP_FAT	GO:0016337~cell-cell adhesion		9.52E–03
GOTERM_BP_FAT	GO:0016481~negative regulation of transcription		1.50E–02
GOTERM_BP_FAT	GO:0019233~sensory perception of pain		2.94E–02
GOTERM_BP_FAT	GO:0021510~spinal cord development		3.46E–02
GOTERM_BP_FAT	GO:0021536~diencephalon development		3.31E–03
GOTERM_BP_FAT	GO:0021537~telencephalon development		5.39E–05
GOTERM_BP_FAT	GO:0021543~pallium development		5.70E–03
GOTERM_BP_FAT	GO:0021953~central nervous system neuron differentiation		5.64E–03
GOTERM_BP_FAT	GO:0021954~central nervous system neuron development		2.94E–02
GOTERM_BP_FAT	GO:0021983~pituitary gland development		3.51E–03
GOTERM_BP_FAT	GO:0030323~respiratory tube development		4.02E–03
GOTERM_BP_FAT	GO:0030324~lung development		9.88E–03
GOTERM_BP_FAT	GO:0030326~embryonic limb morphogenesis		9.87E–03
GOTERM_BP_FAT	GO:0031327~negative regulation of cellular biosynthetic process		1.57E–02
GOTERM_BP_FAT	GO:0031328~positive regulation of cellular biosynthetic process		3.53E–03
GOTERM_BP_FAT	GO:0031644~regulation of neurological system process		2.78E–02
GOTERM_BP_FAT	GO:0032989~cellular component morphogenesis		6.51E–10
GOTERM_BP_FAT	GO:0035107~appendage morphogenesis		1.29E–02
GOTERM_BP_FAT	GO:0035108~limb morphogenesis		1.29E–02
GOTERM_BP_FAT	GO:0035113~embryonic appendage morphogenesis		9.87E–03
GOTERM_BP_FAT	GO:0035239~tube morphogenesis		4.67E–02
GOTERM_BP_FAT	GO:0035295~tube development		9.70E–05
GOTERM_BP_FAT	GO:0042127~regulation of cell proliferation		6.35E–04
GOTERM_BP_FAT	GO:0042416~dopamine biosynthetic process		2.33E–02
GOTERM_BP_FAT	GO:0042692~muscle cell differentiation		3.54E–02
GOTERM_BP_FAT	GO:0043010~camera-type eye development		4.96E–03
GOTERM_BP_FAT	GO:0045165~cell fate commitment		1.15E–06
GOTERM_BP_FAT	GO:0045596~negative regulation of cell differentiation		1.29E–03
GOTERM_BP_FAT	GO:0045597~positive regulation of cell differentiation		2.08E–03
GOTERM_BP_FAT	GO:0045892~negative regulation of transcription, DNA-dependent		5.15E–03
GOTERM_BP_FAT	GO:0045893~positive regulation of transcription, DNA-dependent		1.40E–04
GOTERM_BP_FAT	GO:0045934~negative regulation of nucleobase, nucleoside, nucleotide and nucleic acid metabolic process		3.01E–02
GOTERM_BP_FAT	GO:0045935~positive regulation of nucleobase, nucleoside, nucleotide and nucleic acid metabolic process		8.87E–04
GOTERM_BP_FAT	GO:0045941~positive regulation of transcription		4.21E–04
GOTERM_BP_FAT	GO:0045944~positive regulation of transcription from RNA polymerase II promoter		4.36E–05
GOTERM_BP_FAT	GO:0048514~blood vessel morphogenesis		1.62E–02
GOTERM_BP_FAT	GO:0048598~embryonic morphogenesis		9.61E–03
GOTERM_BP_FAT	GO:0048663~neuron fate commitment		2.83E–03
GOTERM_BP_FAT	GO:0048729~tissue morphogenesis		2.03E–02
GOTERM_BP_FAT	GO:0048732~gland development		1.56E–02
GOTERM_BP_FAT	GO:0048736~appendage development		6.20E–03
GOTERM_BP_FAT	GO:0051094~positive regulation of developmental process		1.43E–03
GOTERM_BP_FAT	GO:0051146~striated muscle cell differentiation		1.56E–02
GOTERM_BP_FAT	GO:0051172~negative regulation of nitrogen compound metabolic process		1.96E–02
GOTERM_BP_FAT	GO:0051173~positive regulation of nitrogen compound metabolic process		1.60E–03
GOTERM_BP_FAT	GO:0051253~negative regulation of RNA metabolic process		5.66E–03

Table 4. (Continued)

Category	Term	Benjamini-corrected p-value	
		Nfia knockout	Nfib knockout
GOTERM_BP_FAT	GO:0051254~positive regulation of RNA metabolic process		1.58E–04
GOTERM_BP_FAT	GO:0051960~regulation of nervous system development		9.57E–05
GOTERM_BP_FAT	GO:0060041~retina development in camera-type eye		2.59E–02
GOTERM_BP_FAT	GO:0060173~limb development		6.20E–03
GOTERM_BP_FAT	GO:0060429~epithelium development		9.74E–03
GOTERM_BP_FAT	GO:0060537~muscle tissue development		1.81E–02
GOTERM_BP_FAT	GO:0060538~skeletal muscle organ development		4.11E–03
GOTERM_BP_FAT	GO:0060541~respiratory system development		9.28E–03

observed *in vitro* (Kruse and Sippel, 1994). However, whether heterodimerisation occurs *in vivo* remains unknown. To investigate whether NFIA and NFIB physically interact in the developing cortex, we performed co-immunoprecipitation of NFIA and NFIB using E13 neocortical lysates (Figure 4(d)). Compared to the input, NFIA and NFIB proteins were enriched in the immunoprecipitate, obtained using antibodies that specifically recognise the other family member, thereby demonstrating that heterodimerisation can occur *in vivo*. Hence, NFIA and NFIB can potentially heterodimerise to co-regulate their target gene expression.

Double heterozygous Nfia;Nfib knockout embryos have similar brain defects to those of single homozygous knockout mice

To test whether the total number of *Nfi* alleles modulates cortical development, we crossed *Nfia* knockout (Das Neves et al., 1999) with *Nfib* conditional (Hsu et al., 2011); *R26-CreERT* (Ventura et al., 2007) mice. Tamoxifen injection at embryonic day E10.5, E11.5 and E12.5 generated *Nfia;Nfib* double heterozygous knockout embryos (hereafter referred to as $Nfia^{+/-}$;$Nfib^{+/-}$). At E18, all $Nfia^{+/-}$;$Nfib^{+/-}$ embryos displayed retention of the interhemispheric fissure and dysgenesis of the corpus callosum as shown by axonal GAP43 staining (Figure 5(a)–(h)). Furthermore, the hippocampi of these embryos showed a distinct malformation, with a reduction in the dentate gyrus, again comparable to the individual null strains (Figure 5(i)–(l)). Hence, the phenotype of the $Nfia^{+/-}$;$Nfib^{+/-}$ embryos was very similar to that of $Nfia^{-/-}$ or $Nfib^{-/-}$ single knockout embryos (Barry et al., 2008; Das Neves et al., 1999; Piper et al., 2009, 2010, 2014; Shu et al., 2003; Steele-Perkins et al., 2005).

On a cellular level, the brains of $Nfia^{+/-}$;$Nfib^{+/-}$ mice displayed a reduction in astroglial cells as assessed by the expression of the mature astroglial marker GFAP, a finding consistent with that observed in single homozygous knockout embryos (Figure 6) (Shu et al., 2003; Steele-Perkins et al., 2005). At the midline, double heterozygous brains showed a reduction in all three glial populations. GFAP expression was completely absent in the glial wedge, as was observed in single $Nfia^{-/-}$ or $Nfib^{-/-}$ embryos (Figure 6(a)–(d)). However, in contrast to single $Nfia^{-/-}$ or $Nfib^{-/-}$ brains, we observed scattered GFAP-positive cells in the vicinity of the midline, which may represent midline zipper glia or indusium griseum glia (Figure 6(a)–(d)). As their presence and locations varied between individual embryos, these cells are likely to represent individual cells that escaped recombination and therefore maintained NFIB expression as previously described (Harris et al., 2016). In single heterozygous knockout embryos, all three glial populations were present, although GFAP expression levels were reduced (Data not shown; Shu et al., 2003; Steele-Perkins et al., 2005). GFAP expression was also reduced in the ammonic neuroepithelium and fimbrial glioepithelium of the hippocampus of $Nfia^{+/-}$;$Nfib^{+/-}$ mice. This phenotype was more reminiscent of $Nfia^{-/-}$ embryos than $Nfib^{-/-}$ embryos, in which GFAP expression was retained to a greater extent in the fimbrial glioepithelium (Figure 6(e)–(h)). Hence, the loss of one allele of both *Nfia* and *Nfib* to a large extent mimics the glial phenotype of homozygous knockout of either family member.

Complete allelic loss of Nfia and Nfib results in a more severe cortical phenotype

The question remains as to whether a further reduction in the number of *Nfia* and *Nfib* alleles would affect corticogenesis. To assess whether loss of both copies of *Nfia* and *Nfib* increase the severity of the developmental brain phenotype, we analysed *Nfia;Nfib* double homozygous knockout embryos at E16. Compared to double heterozygous (Figure 7) or single homozygous knockout embryos (Barry et al., 2008; Das Neves et al., 1999; Piper et al., 2009, 2010; Shu et al., 2003; Steele-Perkins et al., 2005), the phenotype of double homozygous knockout embryos was more severe. In contrast to the other genotypes examined, no GFAP-positive cells were detected at the midline of $Nfia^{-/-}$;$Nfib^{-/-}$ mice (Figure 7(a′)–(c′)), demonstrating a further reduction in glial differentiation in these mice. In the hippocampus, the fimbria of double homozygous knockout animals showed even more prominent decrease in glial differentiation, with no GFAP-positive cells detected (Figure 7(d)–(f)).

The lateral ventricles of these mice were consistently enlarged compared to the other genotypes (Figure 7(a)–(c)) (Steele-Perkins et al., 2005; Das Neves et al., 1999). In conjunction, the ventricular length of both the cingulate cortex and neocortex increased in double knockout embryos, resulting in a near doubling of length in comparison with the wildtype, single knockout and heterozygous double knockout animals (Figure 7(g) and Table 5). Although the overall thickness of the cortex remained unchanged when compared to single knockout or double heterozygous animals, cortical plate thickness was reduced in the medial neocortex (Figure 7(c″ and Table 5). The medial

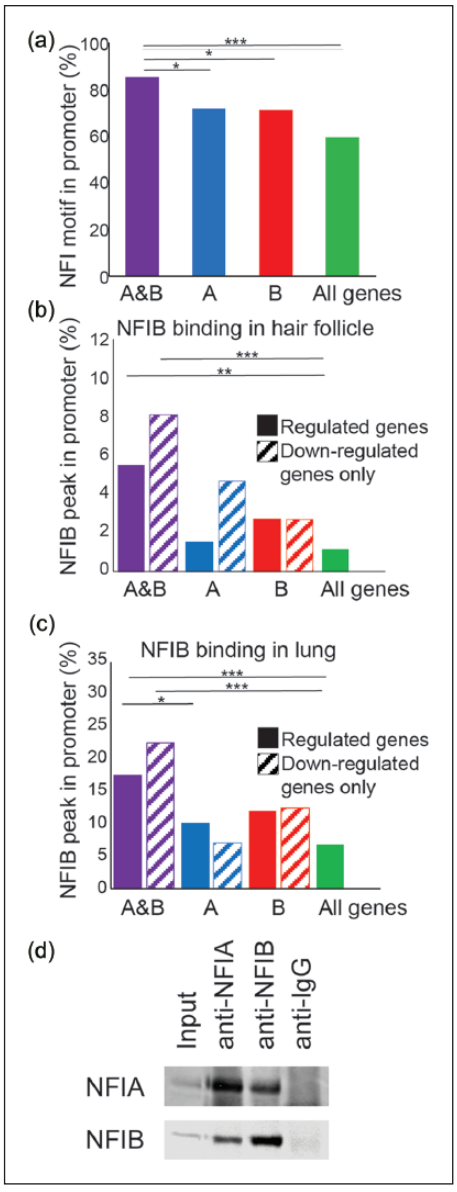

Figure 4. NFIA and NFIB display overlapping regulation.
mRNA sequencing was performed on neocortical tissue dissected from E16 *Nfia* and *Nfib* knockout mice. The 91 shared mis-regulated genes in *Nfia* and *Nfib* knockout mice were enriched for the presence of an NFI binding motif in their promoter, as compared to all genes in the genome, as well as all differentially regulated genes in either *Nfia* or *Nfib* knockout mice (a) Furthermore, the promoter regions of shared mis-regulated genes also displayed an enrichment for putative NFI binding sites, based on an increase in NFIB binding peaks in their promoter observed in ChIP-sequence data from mouse hair follicle stem cells (Chang et al., 2013) and E16 lung tissue (Lajoie et al., 2014) (b and c). This enrichment of putative NFI binding sites was predominantly observed in shared down-regulated genes observed between *Nfia* and *Nfib* knockout mice (striped pattern). Furthermore, NFIA and NFIB can form heterodimers *in vivo*, as both NFIA and NFIB proteins co-immunoprecipitate in nuclear lysate derived from E13 neocortical tissue (d). *<0.05, **<0.005,***<0.001 in a Yates' corrected chi-squared test.

neocortex of double knockout embryos therefore consists of relatively more germinal zone when compared to the lateral neocortex (Figure 7(a)″–(c)″ and Table 5). This change in layer contribution to overall cortical thickness is consistent with the high medial to low lateral expression gradient of NFIA and NFIB (Bunt et al., 2015). The more severe phenotype observed in the medial neocortex, quantified as the ratio of the cortical plate versus the germinal zone, is consistent with higher endogenous NFIA and NFIB expression in the medial neocortex as compared to the lateral neocortex (Figure 7(h) and Table 5). Furthermore, the hippocampal germinal zone was enlarged in double homozygous mice (Figure 7(i)).

Additional staining for the neuronal marker TBR1 revealed that cortical lamination was disrupted within *Nfia*$^{-/-}$;*Nfib*$^{-/-}$ mice, with an apparent absence of the subplate (Figure 8(a)–(c)). We also observed severe perturbations in axon projections within the neocortex (Figure 8(d)–(f)″). No GAP43-positive axons were observed projecting to the midline in *Nfia*$^{-/-}$;*Nfib*$^{-/-}$ mice (Figure 8(f)″) and the white matter within the neocortex was reduced (Figure 8(f)′). The remaining projections observed in the neocortex displayed an abnormal morphology and some ectopically projected to or from the marginal zone. Hence, the lack of both *Nfia* and *Nfib* culminates in cortical phenotypes of increased severity compared to those resulting from individual *Nfi* deletion.

Discussion

This work has revealed that during embryogenesis, NFIA and NFIB function additively to regulate cortical development, as decreasing the number of *Nfi* alleles culminated in a more severe cortical phenotype. This is in line with the overlap of NFIA and NFIB functions in regulating radial glial proliferation and differentiation (Barry et al., 2008; Betancourt et al., 2014; Gobius et al., 2016; Piper et al., 2009, 2010, 2014), with a further reduction in the production of differentiated neural and glial progeny evident when both genes are knocked out.

Whether NFIA and NFIB proteins can fully recapitulate each other's biological function in the radial glia during corticogenesis remains to be further investigated. As not all misregulated genes in the *Nfia* and *Nfib* knockouts overlap, it is not clear whether only the shared misregulated genes are responsible for the observed phenotypes, or whether NFIA and NFIB also uniquely regulate other downstream targets that contribute to the observed phenotype. The latter is complicated as NFIA and NFIB are differentially expressed in the progeny of radial glia. Therefore, the differences in regulated genes detected in our transcriptomic analyses might originate from differentiated cells, rather than from the radial glia themselves. This could explain why the unique NFIA or NFIB targets were not enriched within the VZ datasets. However, the shared down-regulated genes are enriched for direct NFI binding and high expression in the VZ (Tables 1 and 2). For a subset of the potential direct targets in radial glia, such as *Bcan*, *Ccdc80*, *Slc26a7* and *Slc9a3r*, the VZ expression also showed a high caudal to low rostral expression gradient (Allen Institute, 2013; Diez-Roux et al., 2011; Kawaguchi et al., 2008; Visel et al., 2004), similar to NFIA and NFIB (Bunt et al., 2015). Despite this, these potential direct targets might not be sufficient to explain the complete *Nfi* knockout phenotype. For instance, lectican protein BCAN and extracellular matrix glycoprotein tenascin-C (TNC) are implicated with altered radial glial proliferation and differentiation (Garcion et al., 2004), but combined knockout of these genes together with other family members did not result in a severe developmental brain phenotype (Rauch et al., 2005). Nevertheless, these shared down-regulated genes provide a foundation to investigate the role of NFIA and NFIB in radial glial differentiation. Gene expression analyses

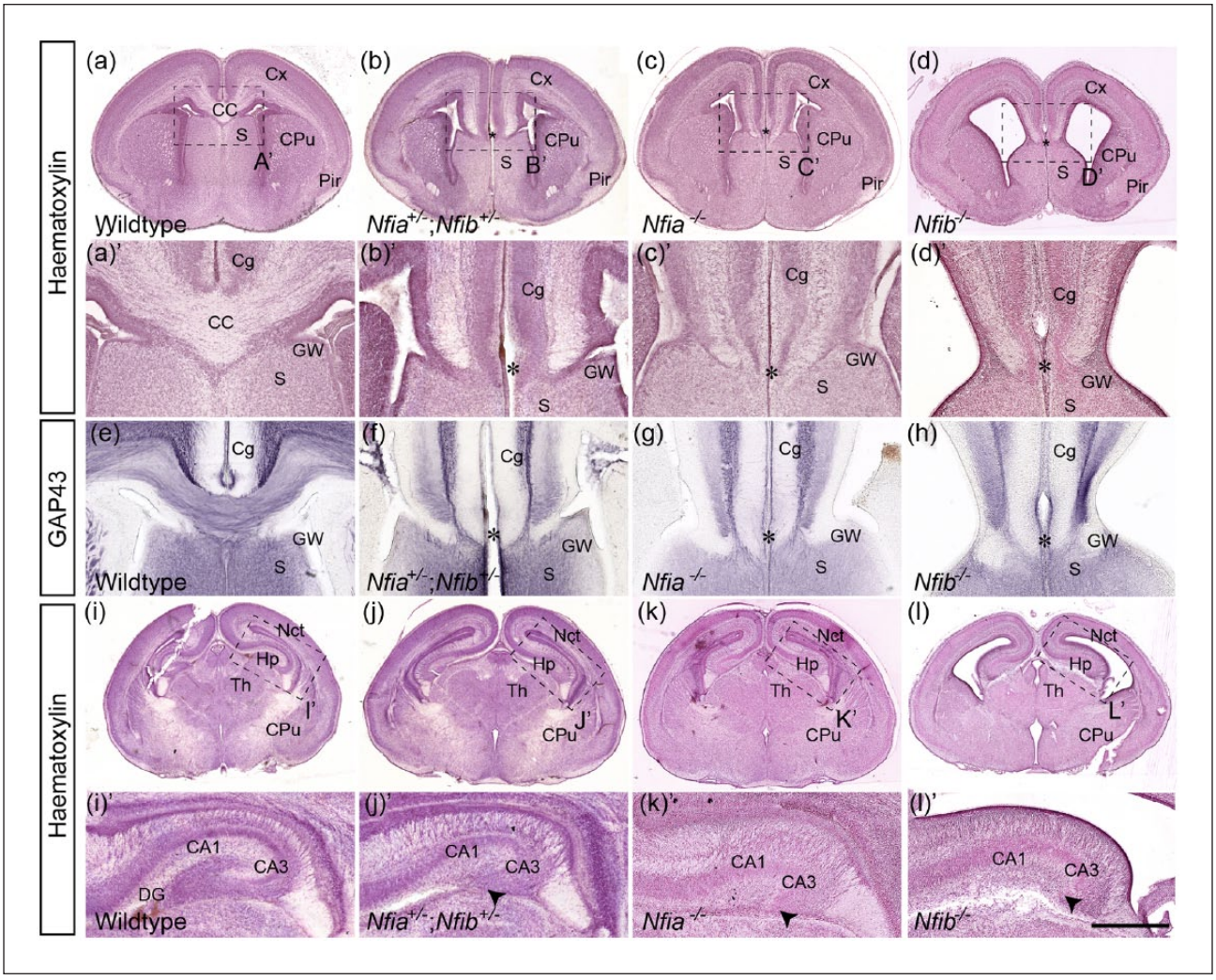

Figure 5. Morphological changes in the cortex of *Nfia*$^{+/-}$;*Nfib*$^{+/-}$ mice are similar to those in single homozygous knockout animals.
Nfia;*Nfib* double heterozygous knockout brains (*Nfia*$^{+/-}$;*Nfib*$^{+/-}$) were generated by tamoxifen administration at E10.5, E11.5 and E12.5 to *Nfia*$^{+/-}$;*Nfib*$^{cond/+}$;R26-CreERT2 pregnant dams . Coronal sections of E18 brains were stained for haematoxylin (a-d, i-l) or GAP43 (e-h). The corpus callosum was clearly evident in wildtype mice (a', e; no arrows in figure). In contrast, *Nfia*$^{+/-}$;*Nfib*$^{+/-}$ mice exhibited retention of the midline fissure and dysgenesis of the corpus callosum (b', f; asterisks). This was similar to *Nfia*$^{-/-}$ (c', g) or *Nfib*$^{-/-}$ (d', h) embryos, where no axonal crossing in rostral coronal sections was observed (c', d', g, h; asterisks). Compared to the wildtype (i'; no arrow in figure), *Nfia*$^{+/-}$;*Nfib*$^{+/-}$ embryos also displayed a reduction in the size of the dentate gyrus (j'; arrowhead), a phenotype also evident in single homozygous embryos (k', l'; arrowheads).
Scale bar (in l'): a -d, i -l = 500 µm; a' -d ', e -h, i' -l' = 125 µm. CC: corpus callosum; Cx: cortex; S: septum; CPu: striatum, Pir: piriform cortex; Cg: cingulate cortex; GW: glial wedge; Nct: neocortex, Hp: hippocampus, Th: thalamus, DG: dentate gyrus; CA1 -3: hippocampal subfields.

using mRNA isolated specifically from the radial glia of *Nfia* and *Nfib* knockout embryos, rather than whole neocortex, will be required to fully dissect the regulated pathway and the potential overlap in targets between the two proteins. The exclusion of other cell types of the neocortex, such as intermediate progenitors, neurons and glia, will provide a more complete picture of both common and distinct functions of these genes, especially if combined with chromatin immunoprecipitation studies to determine direct binding.

In vitro experiments have demonstrated that the DNA-binding motif of both proteins are near identical (Jolma et al., 2013), suggesting that NFIA and NFIB likely bind to the same target genes. However, we cannot rule out that their relative binding affinity may differ *in vivo*. More importantly, the different C-terminal transactivation domains of NFIA and NFIB might vary in how they interact with other proteins and hence how they activate their target genes, thus contributing to the observed differences in our mRNA-sequencing datasets. It is possible that genes that are uniquely misregulated in only one knockout might represent transcriptional targets for which this specific NFI has the strongest DNA binding affinity/specificity or has stronger transcriptional activation. Such genes may still be regulated by the other NFI family member, but due to their lower affinity or activation, the observed regulation may be masked when the other NFI family member is present.

Based on the high similarity of the double heterozygous knockout brains with either single homozygous *Nfia* or *Nfib* knockout brains, we can conclude that in early development,

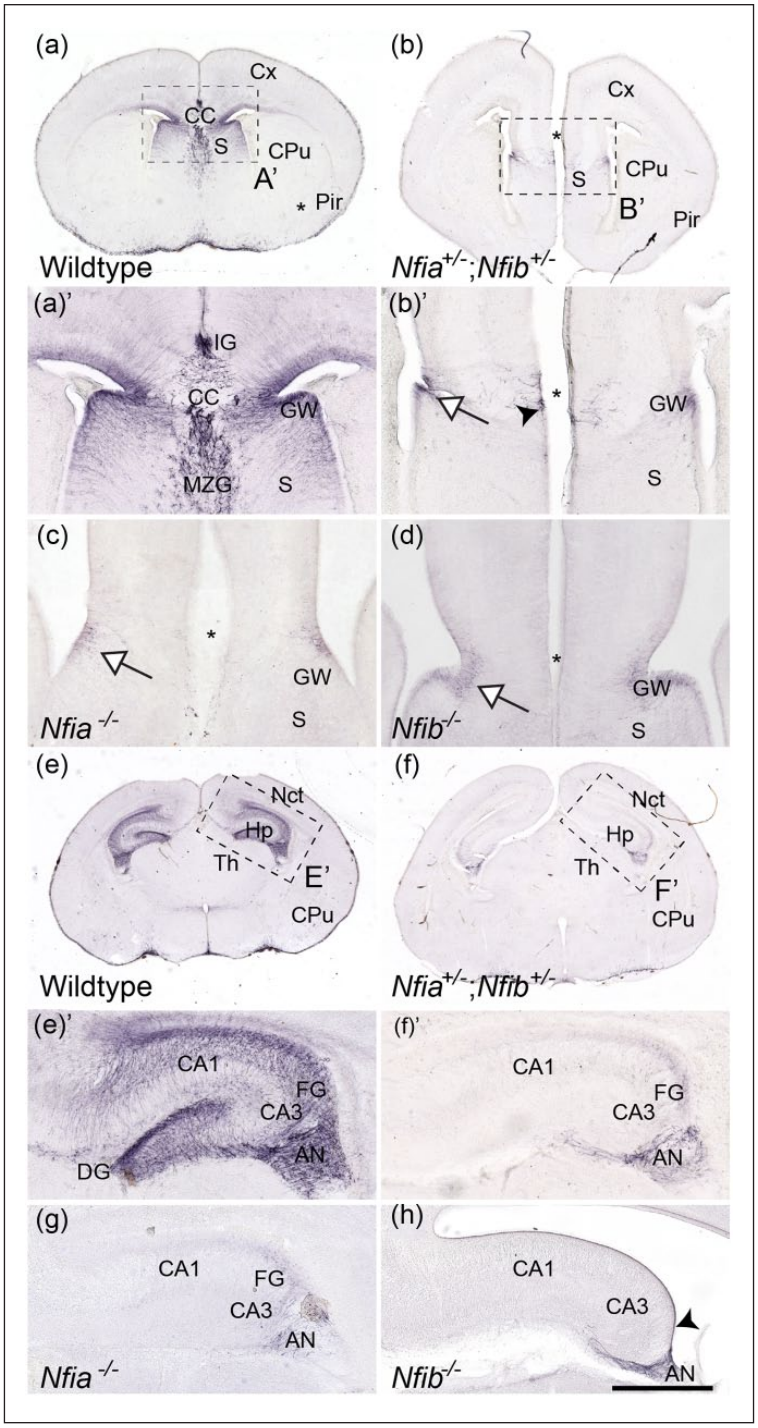

Figure 6. The reduction of cortical astroglia in *Nfia*$^{+/-}$;*Nfib*$^{+/-}$ mice is comparable to that in single homozygous knockout animals. Immunohistochemical staining of E18 coronal sections showing the expression of the astroglial marker GFAP at the midline (a-d) and hippocampus (e-h). In wildtype embryos (A, A'), GFAP expression was detected in the indusium griseum, the glial wedge and the midline zipper glia at the midline, as well as within cortical radial glia. In *Nfia*$^{+/-}$;*Nfib*$^{+/-}$mice (b, B'), GFAP expression was absent in the cortex and reduced at the midline (B'; asterisks). The GFAP-positive glial wedge cell population was reduced (arrow), while only sparse GFAP labelling was detected at the unfused midline (arrow head in B'). This phenotype was comparable to that observed in *Nfia*$^{-/-}$ (c) or *Nfib*$^{-/-}$ (d) mice, in which GFAP immunoreactivity within the indusium griseum glia and midline was absent, and was markedly reduced in the region of the glial wedge (open-headed arrows in C and D). Similarly, GFAP staining was reduced throughout the hippocampus of *Nfia*$^{+/-}$;*Nfib*$^{+/-}$mice (F, F') compared to that in wildtype controls (e, E'). The remaining staining was localized in the ammonic neuroepithelium and fimbrial glioepithelium (F'). This expression pattern was reminiscent of that in *Nfia*$^{-/-}$ mice (g), whereas *Nfib*$^{-/-}$ embryos only retained GFAP immunoreactivity within the fimbrial glioepithelium (arrowhead in h). Scale bar (in H): A, B, E, F = 500 µm; A', B', C, D, E', F', G, H = 125 µm. CC = corpus callosum; Cx = cortex; S = septum; CPu = striatum, Pir = piriform cortex; IG = indusium griseum; GW = glial wedge; MZG = midline zipper glia; Nct = neocortex, Hp = hippocampus, Th = thalamus, DG = dentate gyrus; CA1-3 = hippocampal subfields, AN = ammonic neuroepithelium; FG = fimbrial glioepithelium.

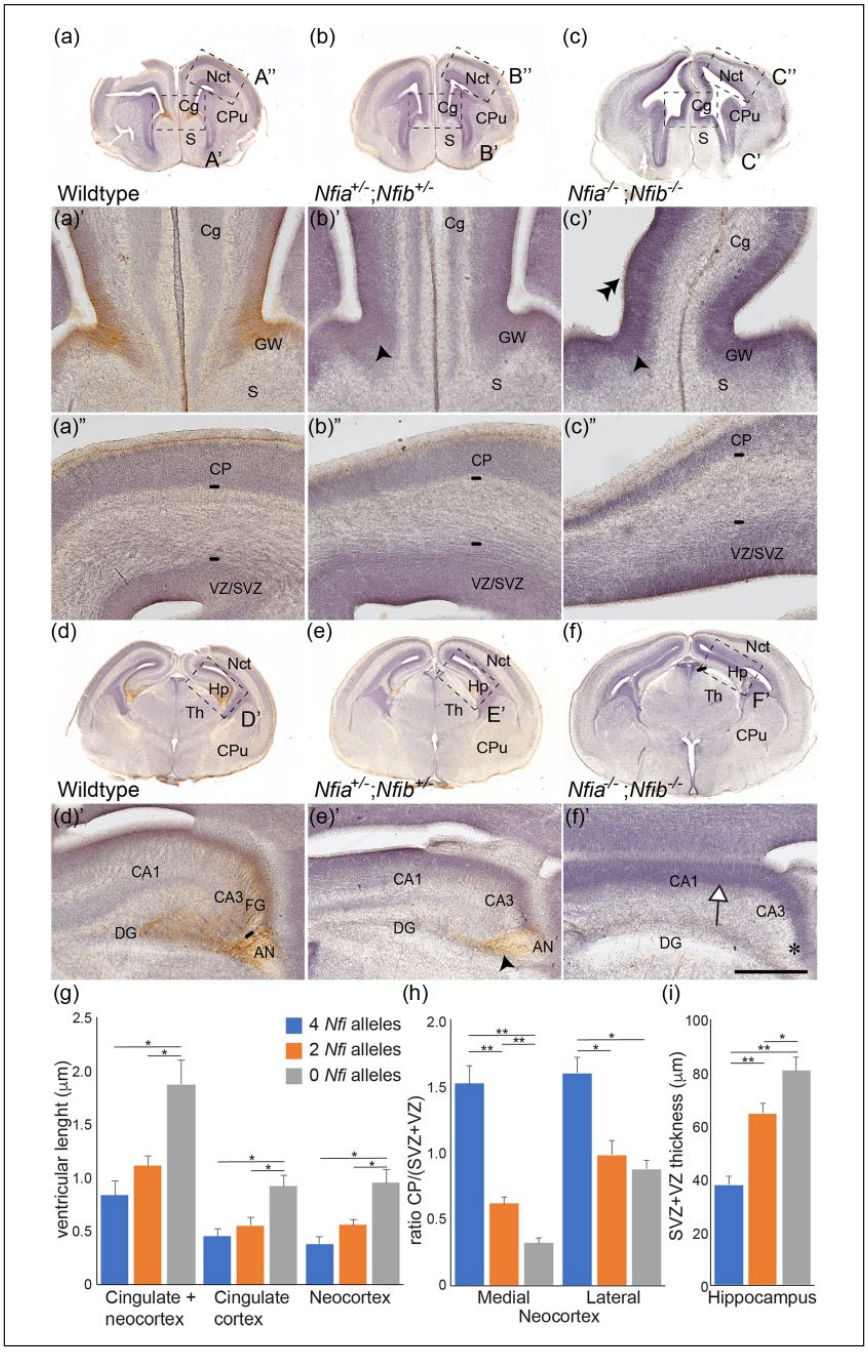

Figure 7. *Nfia*$^{-/-}$;*Nfib*$^{-/-}$ mice display a more severe cortical phenotype compared to *Nfia*$^{+/-}$;*Nfib*$^{+/-}$ mice.

GFAP and haematoxylin staining of E16 coronal brain sections shows that compared to wildtype (a, d) and *Nfia*$^{+/-}$;*Nfib*$^{+/-}$ (b, e) embryos, Nfia$^{-/-}$;Nfib$^{-/-}$mice (c, f) display a more severe cortical phenotype. GFAP expression within the glial wedge of the wildtype was clearly evident at this age (a′), but was diminished/absent in both *Nfia*$^{+/-}$;*Nfib*$^{+/-}$ and *Nfia*$^{-/-}$;*Nfib*$^{-/-}$mice (arrowheads in b′, c′). Moreover, the dorso-ventral expansion of the cingulate cortex in double homozygous knockout mice resulted in the aberrant morphology of this structure (double arrowhead in c′). The cortical plate (CP) of mutant embryos showed a successive reduction in size (compare brackets in a″, b″ and c″), whereas the ventricular/subventricular zones (VZ/SVZ) were larger in the double homozygous knockout mice. Within the hippocampus of wildtype mice at this age (d, d′), GFAP expression was observed in the ammonic neuroepithelium and the fimbrial glioepithelium. GFAP expression was markedly reduced in the hippocampus of *Nfia*$^{+/-}$;*Nfib*$^{+/-}$ mice (arrowhead in e′) and no GFAP expression was evident in the hippocampus of *Nfia*$^{-/-}$;*Nfib*$^{-/-}$mice (asterisk in f′). Moreover, the hippocampal VZ/SVZ of the double homozygous mutant was enlarged (open-headed arrows in f′). Quantification of the ventricular length in sections matched to those represented in (a–c) in three to six animals per condition, revealed an increase in both cingulate and neocortical length of the homozygous double knockout (g). In the neocortex, this increase is also accompanied by a decreased ratio of CP to VZ/SVZ thickness, especially medially (h). The SVZ and VZ thickness also increased in the hippocampus (i).

Scale bar (in f′) a–f = 300 µm; a′–c″, d′–f″ = 80 µm. S: septum; CPu: striatum; Cg: cingulate cortex; GW: glial wedge; CP: cortical plate; VZ/SVZ: germinal zone (ventricular and subventricular zone); Nct: neocortex; Hp: hippocampus; Th: thalamus; DG: dentate gyrus; CA1–3: hippocampal subfields; AN: ammonic neuroepithelium; FG: fimbrial glioepithelium.

*p < 0.05; **p < 0.005 (Student's t-test)

Table 5. Quantification of cortical measurements.

Number of *Nfi* alleles	Radial thickness layers																					
	Ventricular length				Radial thickness				Hippocampus		Medial neocortex				Lateral neocortex							
	Cingulate cortex (µm)		Neocortex (µm)		Cortex (µm)		Cingulate cortex (µm)		Medial neocortex (µm)		Germinal zone (µm)		Cortical plate (µm)		Ratio		Germinal zone (µm)		Cortical plate (µm)		Ratio	
	Average	Standard error	Average	Standard error	Average	Standard error	Average	Standard error	Average	Standard error	Average	Standard error	Average	Standard error	Average	Standard error	Average	Standard error	Average	Standard error	Average	Standard error
4	541.1	90.5	458.4	84.1	999.5	160.4	343.8	27.3	429.3	20.0	37.6	3.4	92.1	5.5	137.3	10.0	1.5	0.1	121.3	11.1	187.1	8.0	1.6	0.1
2	660.4	89.7	667.2	62.9	1327.6	120.7	258.9	27.5	346.6	35.8	64.6	3.8	116.9	19.1	68.2	7.3	0.6	0.0	155.3	12.9	140.7	13.2	1.0	0.1
0	1102.2	121.9	1142.5	146.4	2244.7	265.5	226.0	36.9	352.0	38.8	80.7	5.4	104.8	10.7	32.8	2.6	0.3	0.0	159.3	4.6	139.8	10.0	0.9	0.1
t-test	p-value																					
4 vs 2	0.386		0.082		0.139		0.068		0.080		0.001		0.259		0.001		0.001		0.110		0.026		0.010	
4 vs 0	0.013		0.007		0.008		0.046		0.113		0.001		0.303		0.000		0.001		0.039		0.013		0.006	
2 vs 0	0.025		0.013		0.011		0.497		0.920		0.012		0.641		0.012		0.004		0.827		0.965		0.483	

both NFIA and NFIB function very similarly in corticogenesis and therefore may, in part, compensate for one another when there is a reduction in copy number or functional mutation in one family member. Our data also demonstrate that no specific dimer is essential for cortical development. Although displaying similar phenotypes, in single homozygous knockout mice only NFIA or NFIB homodimers can exist, but in double heterozygous knockouts all homo- and heterodimers can form. Given that double homozygous mice have a more severe phenotype, the different types of dimers seem to function similarly in cortical development.

However, at a later developmental stage, when neurogenesis and gliogenesis are more pronounced, both NFIA and NFIB or specific dimers might function in distinct roles. In the adult brain, mature astrocytes express both NFIA and NFIB, whereas mature oligodendrocytes mainly express NFIA and neurons express NFIB (Chen et al., 2017). *In vitro*, both NFIA and NFIB together with SOX9 are required for astrocytic differentiation from induced pluripotent stem cells (Caiazzo et al., 2015). Furthermore, altering the level of NFIA has also been shown to affect astrocytic and oligodendrocytic gene expression (Glasgow et al., 2014; Wong et al., 2007). Thus, changes in their relative expression might play a more significant role in neurons and glia, at later stages of cortical development and in the adult brain.

Our current lack of knowledge about the regulation of *Nfia* and *Nfib* expression limits our understanding of their role in cerebral development. Why *Nfia* and *Nfib* expression patterns are similar in radial glia, but not in their neuronal and glial progeny, remains unclear. No upstream regulatory transcription factors for *Nfi* have been identified that would explain their initial expression at E12, although their high caudo-medial to low rostro-lateral expression pattern (Bunt et al., 2015) suggests that they are likely to be positively regulated by transcription factors with a similar expression pattern. Alternatively, post-transcriptional regulation could be responsible for this distinct expression gradient. For example, miR-153 (Tsai et al., 2014; Tsuyama et al., 2015) and Drosha (Rolando et al., 2016) have been shown to regulate *Nfi* mRNA levels and translation during neurogenesis. How this similar expression pattern in radial glia subsequently transitions to a cell type-specific glial and neuronal expression remains to be identified.

Due to the perinatal lethality of *Nfia* and *Nfib* knockout mice, as well as the low embryonic viability of $Nfia^{-/-};Nfib^{-/-}$ mice used in our study, these models have limited applicability to determine the progression and functional consequences of the observed phenotype postnatally. Furthermore, these models cannot answer fundamental questions about the differences in function of NFIA and NFIB or their dimers. Brain-specific deletion of both *Nfi* genes using conditional knockout alleles may overcome some of these issues, assuming that double homozygous knockout in the brain has no effect on viability. In theory, utilising the recent generation of a conditional *Nfib* overexpression model (Semenova et al., 2016) crossed to an *Nfia* knockout mouse would be able to demonstrate whether increasing NFIB protein levels could compensate for the absence of *Nfia*. However, this would require ectopic NFIB expression to mimic both the expression level and temporal and spatial specificity of NFIA. A better approach would be a knock in of *Nfia* into the *Nfib* locus or vice versa, although this might cause problems in other tissues where a specific family member might be required.

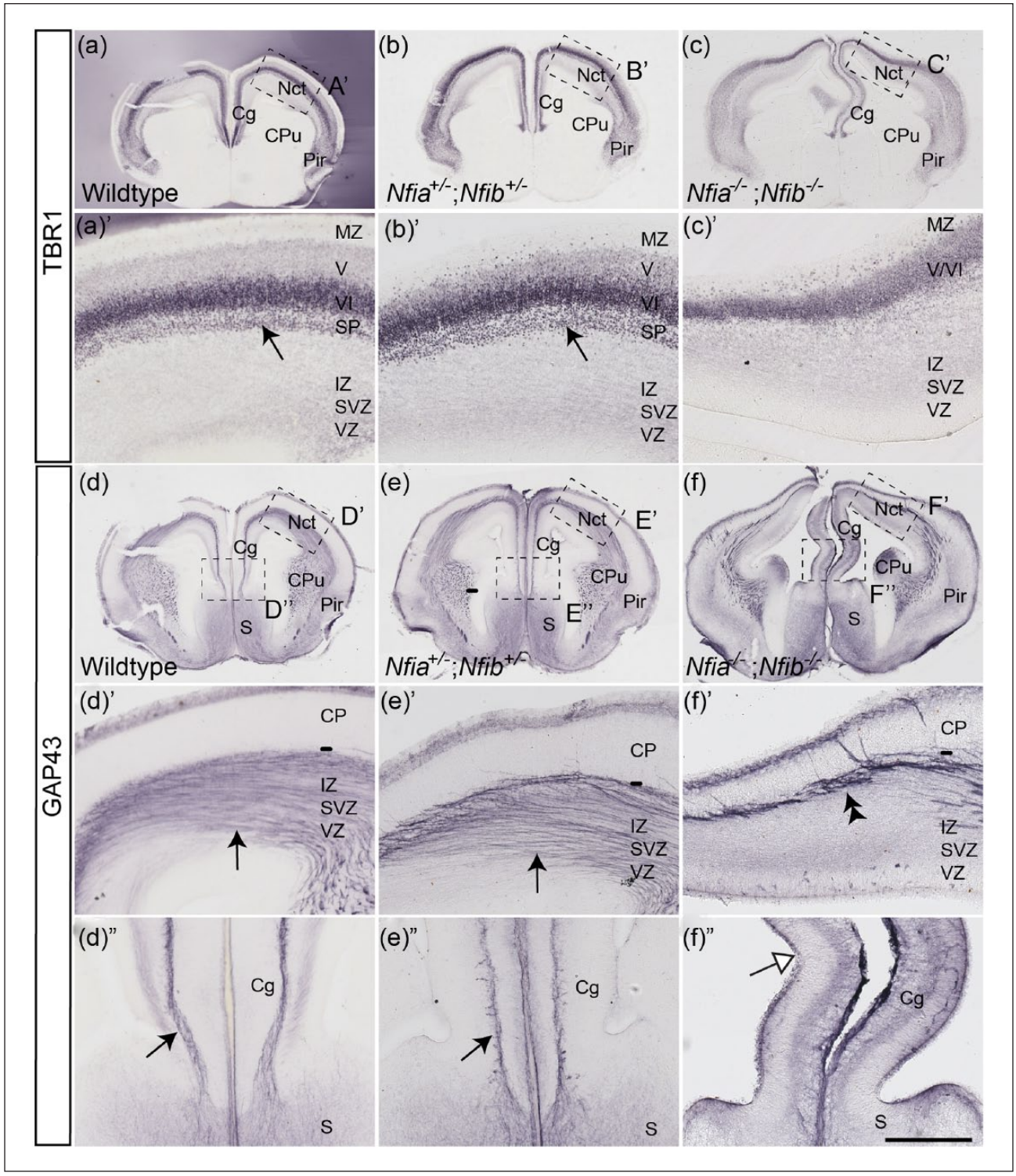

Figure 8. Double knockout of *Nfia* and *Nfib* results in a reduction of neurons and axonal projections within the cerebral cortex.
Coronal sections of wildtype (a, d), *Nfia*$^{+/-}$;*Nfib*$^{+/-}$ (b, e) and *Nfia*$^{-/-}$;*Nfib*$^{-/-}$ (c, f) mice at E16 stained for TBR1 (a–c) and GAP43 (d–f). Within the neocortex, the subplate was visible within wildtype and *Nfia*$^{+/-}$;*Nfib*$^{+/-}$ mice (arrows in a′ and b′). However, no subplate was evident within *Nfia*$^{-/-}$;*Nfib*$^{-/-}$ mice at this age (c′). There were also fewer TBR1-expressing cortical neurons present within *Nfia*$^{-/-}$;*Nfib*$^{-/-}$ mice at this age compared to that in wildtype and *Nfia*$^{+/-}$;*Nfib*$^{+/-}$ mice. GAP43 staining revealed extensive axonal projections within the neocortex of wildtype and *Nfia*$^{+/-}$;*Nfib*$^{+/-}$ mice (arrows in d′ and e′), some of which extended into the cingulate cortex (arrows in d″ and e″). In *Nfia*$^{-/-}$;*Nfib*$^{-/-}$mice, few GAP43-expressing axons were seen within the neocortex (double arrowhead in f′), and none were observed within the cingulate cortex (f″). Moreover, some ectopic axonal projections were observed in the marginal zone of *Nfia*$^{-/-}$;*Nfib*$^{-/-}$ mice.
Scale bar (in f″) a–f = 300 μm; a′–c′, d′–f″ = 80 μm. Nct: neocortex; S: septum; CPu: striatum; MZ: marginal zone; V, VI: cortical layers V and VI; IZ: intermediate zone; SVZ: subventricular zone; VZ: ventricular zone; CP: cortical plate; Cg: cingulate cortex; SP: subplate; Pir: piriform cortex.

The question remains whether NFIA and NFIB have only overlapping functions in regulating radial glial proliferation and differentiation or whether they also have yet unknown distinct roles in this cell type. If they function interchangeably in radial glia, their combined expression might provide a more precise mechanism to regulate the balance between proliferation and differentiation. As we show that loss of NFI results in a dosage-dependent cortical defect, maintaining the correct protein levels is essential for normal cortical development. In conclusion, our work demonstrates that NFIA and NFIB function additively in the context of early cerebral development, as the combined allelic loss of these genes directly correlates with the severity of the developmental brain phenotypes.

Acknowledgements

The authors thank the staff of the University of Queensland Biological Resources (UQBR) animal facility, the QBI Advanced Microscopy and Analysis Facility and the QBI Centre for Brain Genomics for their expertise and assistance in this project. The authors are grateful to Rowan Tweedale for her critical comments on the manuscript.

Declaration of conflicting interests

The author(s) declared no potential conflicts of interest with respect to the research, authorship and/or publication of this article.

Funding

This work was supported by National Health and Medical Research Council project grants (GNT1057751 to M.P. and GNT1100443 to L.J.R.), Australian Research Council Discovery Grants (DP160100368 to M.P. and DP140101499 to L.J.R.) and NYSTEM grants (C026429 and C030133 to R.M.G.). M.P. was supported by a fellowship (Australian Research Council Future Fellowship; FT120100170). L.J.R. was supported by an NHMRC Principal Research Fellowship. D.V., J.W.C.L. and L.H. were supported by an Australian Government Research Training Program Scholarship. J.W.C.L. was supported by an UQ Centennial Scholarship. Y.Y. was supported by the Aleks Brumby Summer Research Scholarship. The funders had no role in study design, data collection and analysis, decision to publish, or preparation of the manuscript. The content is solely the responsibility of the authors and does not necessarily represent the official views of the funders.

References

Allen Institute for Brain Science. Allen Developing Mouse Brain Atlas [Internet]. (2013) Available at: http://developingmouse.brain-map.org. (accessed 1 June 2017).

Barry G, Piper M, Lindwall C, et al. (2008) Specific glial populations regulate hippocampal morphogenesis. *The Journal of Neuroscience* 28(47): 12328–12340.

Betancourt J, Katzman S and Chen B (2014) Nuclear factor one B regulates neural stem cell differentiation and axonal projection of corticofugal neurons. *The Journal of Comparative Neurology* 522(1): 30.

Brun M, Coles JE, Monckton EA, et al. (2009) Nuclear factor I regulates brain fatty acid-binding protein and glial fibrillary acidic protein gene expression in malignant glioma cell lines. *Journal of Molecular Biology* 391(2): 282–300.

Bunt J, Hasselt NE, Zwijnenburg DA, et al. (2012) OTX2 directly activates cell cycle genes and inhibits differentiation in medulloblastoma cells. *International Journal of Cancer* 131(2): E21–E32.

Bunt J, Lim JW, Zhao L, et al. (2015) PAX6 does not regulate Nfia and Nfib expression during neocortical development. *Scientific Reports* 5: 10668.

Caiazzo M, Giannelli S, Valente P, et al. (2015) Direct conversion of fibroblasts into functional astrocytes by defined transcription factors. *Stem Cell Reports* 4(1): 25–36.

Campbell CE, Piper M, Plachez C, et al. (2008) The transcription factor Nfix is essential for normal brain development. *BMC Developmental Biology* 8: 52.

Cebolla B and Vallejo M (2006) Nuclear factor-I regulates glial fibrillary acidic protein gene expression in astrocytes differentiated from cortical precursor cells. *Journal of Neurochemistry* 97(4): 1057–1070.

Chang CY, Pasolli HA, Giannopoulou EG, et al. (2013) NFIB is a governor of epithelial-melanocyte stem cell behaviour in a shared niche. *Nature* 495(7439): 98–102.

Chen KS, Harris L, Lim JW, et al. (2017) Differential neuronal and glial expression of nuclear factor I proteins in the cerebral cortex of adult mice. *The Journal of Comparative Neurology* 525(11): 2465–2483.

Das Neves L, Duchala CS, Tolentino-Silva F, et al. (1999) Disruption of the murine nuclear factor I-A gene (Nfia) results in perinatal lethality, hydrocephalus, and agenesis of the corpus callosum. *Proceedings of the National Academy of Sciences of the United States of America* 96(21): 11946–11951.

Deneen B, Ho R, Lukaszewicz A, et al. (2006) The transcription factor NFIA controls the onset of gliogenesis in the developing spinal cord. *Neuron* 52(6): 953–968.

Diez-Roux G, Banfi S, Sultan M, et al. (2011) A high-resolution anatomical atlas of the transcriptome in the mouse embryo. *PLoS Biology* 9(1): e1000582.

Fane ME, Chhabra Y, Hollingsworth DE, et al. (2017) NFIB mediates BRN2 driven melanoma cell migration and invasion through regulation of EZH2 and MITF. *EBioMedicine* 16: 63–75.

Fietz SA, Lachmann R, Brandl H, et al. (2012) Transcriptomes of germinal zones of human and mouse fetal neocortex suggest a role of extracellular matrix in progenitor self-renewal. *Proceedings of the National Academy of Sciences of the United States of America* 109(29): 11836–11841.

Garcion E, Halilagic A, Faissner A, et al. (2004) Generation of an environmental niche for neural stem cell development by the extracellular matrix molecule tenascin C. *Development* 131(14): 3423–3432.

Glasgow SM, Laug D, Brawley VS, et al. (2013) The miR-223/nuclear factor I-A axis regulates glial precursor proliferation and tumorigenesis in the CNS. *The Journal of Neuroscience* 33(33): 13560–13568.

Glasgow SM, Zhu W, Stolt CC, et al. (2014) Mutual antagonism between Sox10 and NFIA regulates diversification of glial lineages and glioma subtypes. *Nature Neuroscience* 17(10): 1322–1329.

Gobius I, Morcom L, Suarez R, et al. (2016) Astroglial-mediated remodeling of the interhemispheric midline is required for the formation of the corpus callosum. *Cell Reports* 17(3): 735–747.

Grabowska MM, Elliott AD, DeGraff DJ, et al. (2014) NFI transcription factors interact with FOXA1 to regulate prostate-specific gene expression. *Molecular Endocrinology* 28(6): 949–964.

Grant CE, Bailey TL and Noble WS (2011) FIMO: Scanning for occurrences of a given motif. *Bioinformatics* 27(7): 1017–1018.

Gronostajski RM (2000) Roles of the NFI/CTF gene family in transcription and development. *Gene* 249(1–2): 31–45.

Gronostajski RM, Adhya S, Nagata K, et al. (1985) Site-specific DNA binding of nuclear factor I: Analyses of cellular binding sites. *Molecular and Cellular Biology* 5(5): 964–971.

Harris L, Zalucki O, Gobius I, et al. (2016) Transcriptional regulation of intermediate progenitor cell generation during hippocampal development. *Development* 143(24): 4620–4630.

Hsu YC, Osinski J, Campbell CE, et al. (2011) Mesenchymal nuclear factor I B regulates cell proliferation and epithelial differentiation during lung maturation. *Developmental Biology* 354(2): 242–252.

Huang da W, Sherman BT and Lempicki RA (2009a) Bioinformatics enrichment tools: Paths toward the comprehensive functional analysis of large gene lists. *Nucleic Acids Research* 37(1): 1–13.

Huang da W, Sherman BT and Lempicki RA (2009b) Systematic and integrative analysis of large gene lists using DAVID bioinformatics resources. *Nature Protocols* 4(1): 44–57.

Jolma A, Yan J, Whitington T, et al. (2013) DNA-binding specificities of human transcription factors. *Cell* 152(1–2): 327–339.

Kawaguchi A, Ikawa T, Kasukawa T, et al. (2008) Single-cell gene profiling defines differential progenitor subclasses in mammalian neurogenesis. *Development* 135(18): 3113–3124.

Kilpatrick DL, Wang W, Gronostajski R, et al. (2012) Nuclear factor I and cerebellar granule neuron development: An intrinsic-extrinsic interplay. *Cerebellum* 11(1): 41–49.

Kim D, Pertea G, Trapnell C, et al. (2013) TopHat2: Accurate alignment of transcriptomes in the presence of insertions, deletions and gene fusions. *Genome Biology* 14(4): R36.

Klenova E, Chernukhin I, Inoue T, et al. (2002) Immunoprecipitation techniques for the analysis of transcription factor complexes. *Methods* 26(3): 254–259.

Koehler U, Holinski-Feder E, Ertl-Wagner B, et al. (2010) A novel 1p31.3p32.2 deletion involving the NFIA gene detected by array CGH in a patient with macrocephaly and hypoplasia of the corpus callosum. *European Journal of Pediatrics* 169(4): 463–468.

Kruse U and Sippel AE (1994) Transcription factor nuclear factor I proteins form stable homo- and heterodimers. *FEBS Letters* 348(1): 46–50.

Lajoie M, Hsu YC, Gronostajski RM, et al. (2014) An overlapping set of genes is regulated by both NFIB and the glucocorticoid receptor during lung maturation. *BMC Genomics* 15: 231.

Leegwater PA, van Driel W and van der Vliet PC (1985) Recognition site of nuclear factor I, a sequence-specific DNA-binding protein from HeLa cells that stimulates adenovirus DNA replication. *The EMBO Journal* 4(6): 1515–1521.

Lim JW, Donahoo AL, Bunt J, et al. (2015) EMX1 regulates NRP1-mediated wiring of the mouse anterior cingulate cortex. *Development* 142(21): 3746–3757.

Lu W, Quintero-Rivera F, Fan Y, et al. (2007) NFIA haploinsufficiency is associated with a CNS malformation syndrome and urinary tract defects. *PLoS Genetics* 3(5): e80.

Negishi Y, Miya F, Hattori A, et al. (2015) Truncating mutation in NFIA causes brain malformation and urinary tract defects. *Human Genome Variation* 2: 15007.

Perez-Casellas LA, Wang X, Howard KD, et al. (2009) Nuclear factor I transcription factors regulate IGF binding protein 5 gene transcription in human osteoblasts. *Biochimica et Biophysica Acta* 1789(2): 78–87.

Piper M, Barry G, Harvey TJ, et al. (2014) NFIB-mediated repression of the epigenetic factor Ezh2 regulates cortical development. *The Journal of Neuroscience* 34(8): 2921–2930.

Piper M, Barry G, Hawkins J, et al. (2010) NFIA controls telencephalic progenitor cell differentiation through repression of the Notch effector Hes1. *The Journal of Neuroscience* 30(27): 9127–9139.

Piper M, Moldrich RX, Lindwall C, et al. (2009) Multiple non-cell-autonomous defects underlie neocortical callosal dysgenesis in Nfib-deficient mice. *Neural Development* 4: 43.

Plachez C, Lindwall C, Sunn N, et al. (2008) Nuclear factor I gene expression in the developing forebrain. *The Journal of Comparative Neurology* 508(3): 385–401.

Rauch U, Zhou XH and Roos G (2005) Extracellular matrix alterations in brains lacking four of its components. *Biochemical and Biophysical Research Communications* 328(2): 608–617.

Rolando C, Erni A, Grison A, et al. (2016) Multipotency of adult hippocampal NSCs *in vivo* is restricted by drosha/NFIB. *Cell stem cell* 19(5): 653–662.

Sajan SA, Fernandez L, Nieh SE, et al. (2013) Both rare and copy number variants are prevalent in agenesis of the corpus callosum but not in cerebellar hypoplasia or polymicrogyria. *PLoS Genetics* 9(10): e1003823.

Semenova EA, Kwon MC, Monkhorst K, et al. (2016) Transcription factor NFIB Is a driver of small cell lung cancer progression in mice and marks metastatic disease in patients. *Cell Reports* 16(3): 631–643.

Shimogori T, Lee DA, Miranda-Angulo A, et al. (2010) A genomic atlas of mouse hypothalamic development. *Nature Neuroscience* 13(6): 767–775.

Shu T, Butz KG, Plachez C, et al. (2003) Abnormal development of forebrain midline glia and commissural projections in Nfia knock-out mice. *The Journal of Neuroscience* 23(1): 203–212.

Steele-Perkins G, Plachez C, Butz KG, et al. (2005) The transcription factor gene Nfib is essential for both lung maturation and brain development. *Molecular and Cellular Biology* 25(2): 685–698.

Trapnell C, Williams BA, Pertea G, et al. (2010) Transcript assembly and quantification by RNA-Seq reveals unannotated transcripts and isoform switching during cell differentiation. *Nature Biotechnology* 28(5): 511–515.

Tsai PC, Bake S, Balaraman S, et al. (2014) MiR-153 targets the nuclear factor-1 family and protects against teratogenic effects of ethanol exposure in fetal neural stem cells. *Biology Open* 3(8): 741–758.

Tsuyama J, Bunt J, Richards LJ, et al. (2015) MicroRNA-153 regulates the acquisition of gliogenic competence by neural stem cells. *Stem Cell Reports* 5(3): 9.

Ventura A, Kirsch DG, McLaughlin ME, et al. (2007) Restoration of p53 function leads to tumour regression *in vivo*. *Nature* 445(7128): 661–665.

Visel A, Thaller C and Eichele G (2004) GenePaint.org: An atlas of gene expression patterns in the mouse embryo. *Nucleic Acids Research* 32(Database issue): D552–D556.

Waki H, Nakamura M, Yamauchi T, et al. (2011) Global mapping of cell type-specific open chromatin by FAIRE-seq reveals the regulatory role of the NFI family in adipocyte differentiation. *PLoS Genetics* 7(10): e1002311.

Wang W, Crandall JE, Litwack ED, et al. (2010) Targets of the nuclear factor I regulon involved in early and late development of postmitotic cerebellar granule neurons. *Journal of Neuroscience Research* 88(2): 258–265.

Wang W, Mullikin-Kilpatrick D, Crandall JE, et al. (2007) Nuclear factor I coordinates multiple phases of cerebellar granule cell development via regulation of cell adhesion molecules. *The Journal of Neuroscience* 27(23): 6115–6127.

Wong YW, Schulze C, Streichert T, et al. (2007) Gene expression analysis of nuclear factor I-A deficient mice indicates delayed brain maturation. *Genome Biology* 8(5): R72.